THE UNIVERSITY OF
WARWICK

NAME: **Shin Yiing Lim**
YEAR: **4** INTAKE YEAR**: 2012**
TYPE OF PROJECT: **CH401/410 Research Project**
TITLE: **Protein Conjugated Gold Nanoparticles Biosensors**
SUPERVISOR: **Prof. Matthew I. Gibson**
NUMBER OF WORDS: **8470 words**

Abstract

Protein mediated interactions are one of the most important interactions in biological systems. The detection of protein-protein interactions remains an interesting topic of research as several infections and diseases begin with the simple docking of antigens or recognition of foreign molecules in the body. The rapid development in nanotechnology in the past decades provides a great platform in using nanoscale materials in this area of medicine. The architecture and engineering of nanoparticles as biosensors have been an important topic of research. As such, this report offers insights into the development of a rational, simple and scalable protein-gold nanoparticle bioconjugate to modulate cellular interactions and act as a biosensor.

Adopting the covalent coupling method that uses the common preactivation method using water soluble 1-ethyl-3-(3-dimethylaminopropyl)carbodiimide hydrochloride (EDC) and *N*-hydroxysuccinimide (NHS), a controlled and stable, yet simple technique of immobilisation of proteins was tested. This conjugation method was chosen due to its simplicity in procedure, accessibility to materials and potential for large-scale production. PEG-2-mercaptoethyl ether acetic acid, a thiolated PEG polymer chain with carboxylate group was used as a spacer and stabiliser of the nanoparticle to increase colloidal stability and at the same time used as a bridge to form a well-defined protein-linker-AuNP bioconjugate.

Ultimately, the protein-functionalised AuNPs were used as nanotools to monitor biological interactions namely attachment onto glycosylated surfaces and antigen detection.

Acknowledgements

I would like to thank my supervisor, Professor Matthew Gibson for providing the opportunity to undertake a rewarding and challenging research project in the lab, and for always giving support and guidance throughout the placement. His enthusiasm and endless knowledge has been a great source of motivation.

Special mention to my mentor, Lucienne Otten for her constant guidance and assistance throughout my placement. Thank you for the advice and support, and for always willing to give your time to help.

Finally, a big thank you to all members of the Gibson research group who have been very accepting and wonderful colleagues. It has been great pleasure to work with everyone in a warm and friendly environment.

List of Abbreviations

Ab	Antibody
AuNP	Gold nanoparticle
BSA	Albumin from bovine serum
Con A	Concanavalin A
DBA	*Dolichos biflorus* agglutinin
EDC	1-Ethyl-3-(3-dimethylaminopropyl)carbodiimide hydrochloride
Fab	Antigen binding region of antibody
Fc	Fragment crystallisable region of antibody
GalNAc	*N*-Acetylgalactosamine
hCG	Human chorionic gonadotropin
Igs	Immunoglobulins
IgG	Immunoglobulin G
IR	Infrared spectroscopy
MES	2-(*N*-morpholino)ethanesulfonic acid
NHS	*N*-hydroxysuccinimide
PBS	Phosphate-buffered saline
PEG	Polyethylene glycol
PNA	Peanut agglutinin from *Arachis hypogea*
PPI	Protein-protein interactions
PPTT	Plasmonic photothermal therapy
RT	Room temperature
SEM	Scanning electron microscopy
SPR	Surface plasmon resonance
TAP-MS	Tandem affinity purification and mass spectrometry
TEM	Transmission electron microscopy
TGA	Thermogravimetric analysis
TNF	Tumour necrosis factor
UV/Vis	Ultraviolet/Visible spectroscopy
XPS	X-ray photoelectron spectroscopy analysis
Y2H	Yeast two-hybrid assays

Content Page

1. Introduction

1.1 Biomolecular Interactions

Biomolecular interactions dictate activity of molecular complexes and binding events in biological systems.[1 - 3] To understand life processes at the molecular level, it is cardinal to first understand these interactions. One of the most important classes of biomolecular interactions is protein-mediated interactions where the reciprocal relationship between proteins and other biomolecules becomes prominent. Proteins are known as the 'workhorses' of the body. Implicitly, all cellular mechanisms of living things revolve around the binding of two or more proteins. The most basal protein mediated interaction could be seen in the binding between enzyme and substrate molecules in catalytic biochemical reactions. Other critical examples in cellular processes include the transduction of signals of the nervous system, regulation of gene expression, cell metabolism and also the control of the cell cycle.[2, 3]

1.2 Protein-Mediated Interactions

Protein-protein interactions (PPI) are defined as the physical docking of molecules onto proteins through non-covalent interactions like hydrophobic contacts, hydrogen bonds and electrostatic interactions.[1 - 3] Covalent interactions do occur through sharing of electrons or disulfide bonds, but are typically rare.[2] Conventional examples of PPI can be seen in the relationship of complexes like enzyme-inhibitor and antibody-antigen. The interactions mediated by proteins differ in structural and functional features like their affinity, composition and lifespan of the association.[3] Usually the effects of PPI are measurable through their biological effects like; the kinetic properties of enzymes, the inactivation or denaturation of a protein or the regulatory role of the protein in an upstream or downstream event.[2] These interactions are characterised by three factors; strength of interaction which involves a stable or transient interaction, specificity which indicates the specific binding of interacting partners and the type of interacting subunits which leads to the formation of homo-oligomer or hetero-oligomer structures.

1.2.1 Monitoring Protein-Mediated Interactions

As PPI is fundamental to most cellular processes, the potential this subject has as a therapeutic target is obvious. The analysis of protein-mediated interactions may reveal unique and serendipitous functional roles for common proteins which could be adopted into other applications. Monitoring and measuring PPI have since been studied extensively by various experimental methods.[2, 4] There are several techniques to detect these interactions and the most common and established high-throughput methods are yeast two-hybrid assays (Y2H) and tandem affinity purification and mass spectrometry (TAP-MS).[4, 5] The former provides a mean to identify direct, transient and unstable PPI through the activation of the expression of reporter genes by transcription factors when the bait and prey proteins come together.[6, 7] The latter requires a biochemical isolation of stable protein complexes, followed by the identification of the protein moieties using mass spectrometry.[6, 8] These two approaches are particularly useful for detection of PPI *in vivo*.

While the traditional methods appear to be relevant, there are some drawbacks in these techniques. Commonly, a combination of these methods is required to corroborate

and confirm protein interactions as no one approach gives a certain result. The Y2H screens have been known to show poor reliability in their results, with high false positive and negative rates of up to 70 %.[9] The poor results are typically due to the nature of the screen, of which the analysis of proteins must take place in the nucleus rather than in local compartments. Furthermore, the use of yeast as a host for the assay may lead to false results as essential post-translational modification of non-yeast proteins may not be feasible. Although TAP-MS gives better accuracy in the results, the purification technique means it is not suitable for loosely associated protein complexes.[1, 2] Transient protein complexes can be easily washed away during purification hence compromising the accuracy of the analysis. There may also be risk of interference on complex formation due to the tagging technique employed. Assuredly, there is an urgent need to develop a method to monitor and measure PPI.

1.3 Nanotechnology for Molecular Interactions

1.3.1 Gold Nanoparticles

Nanotechnology has been under the spotlight for several decades now, and has shown great promise in revolutionising the biomedical field. Defined as the manipulation of matter on a nanoscopic scale, works on the amalgamation of nanotechnology in monitoring molecular interactions are essential in producing the next-generation biomedical tools.

Gold is a valuable precious metal that has been recognised for its therapeutic and decorative applications since ancient times. Gold nanoparticles (AuNPs) have garnered great interest since 1857 when Faraday first reported and characterised the red colour as the colloidal nature of AuNPs.[41] This colouration is due to an optical phenomenon called localised plasmon resonance which occurs when a light wave is trapped within conductive nanoparticles smaller than the wavelength of light.[46 – 48] This leads to a collective oscillation of conduction band electrons of the gold core at a resonant frequency. The optical properties of nanoparticles are governed by several factors including size, shape, degree of aggregation and medium of dispersion (Table 1.1). AuNPs of a size range of 10 to 100 nm appear to be red, but turn blue or colourless upon aggregation. This interesting optical property contributes to a greater significance onto AuNPs.

Diameter of AuNP (nm)	SPR peak, λ_{max} (nm)	Extinction coefficient (M^{-1} cm^{-1})
20	524	9.21×10^{8}
40	530	8.42×10^{9}
60	540	3.07×10^{10}
80	553	7.70×10^{10}
100	572	1.57×10^{11}

Table 1.1. The surface plasmon resonance (SPR) peak and extinction coefficient of gold nanoparticles with different diameter. Optical properties of AuNPs change with the size. [65]

A new milestone was reached when the first method of synthesis of AuNPs was developed. This method, known as the citrate reduction method, was introduced by Turkevich *et al*. in 1951.[42] Since then, several other methods have been developed which allow the controlled synthesis of AuNPs, including the Brust method,[43] Perrault method[44] and Martin method.[45] These modern synthetic approaches opened doors to designing AuNPs of desired size, shape and surface chemistry. One of the greatest breakthroughs in the combination of nanotechnology and molecular biology is the introduction of a reversible method in assembling colloidal AuNPs into aggregates using DNA oligonucleotides by Mirkin *et al*.[10] The preparation of the bioconjugates involves a simple chemisorption of non-complementary DNA oligonucleotides capped with thiol groups, which have high affinity towards gold, onto the surfaces of the AuNPs. The bioconjugated AuNPs were then added to a solution with oligonucleotide duplexes with complementary "sticky ends" to the grafted sequences. The self-assembly of the nanoparticles into macroscopic aggregates were observed proving the efficacy of this straightforward technique. Today, the application of DNA-AuNP bioconjugates have expanded in the biomedical field as; antisense agents for intracellular gene regulation,[11, 12] RNA visualising probes as nanoflares[13] and as an ultrasensitive tool in bio-barcode assays[14] due to their unique physical and optical properties.

1.3.2 Antibody-Functionalised Gold Nanoparticles

Another product of nanotechnology coupled with molecular biology is the commercial antibody-functionalised AuNP known as "Immunogold", which was discovered by Faulk and Taylor in 1971.[15] It was first used as a probe to identify the *Salmonella* antigen under electron microscopy[15] and has since been adopted as a staining reagent for transmission electron microscopy (TEM).[16] When enhanced with silver, the antibody-AuNP (Ab-AuNP) bioconjugates can not only be used for brightfield microscopy, but also for scanning electron microscopy (SEM) due to the increase in particle size.[16, 17] The preparation of "Immunogold" is simple, quick and economical, which involves a direct physisorption of antibodies (Abs) onto the surface of AuNPs, usually less than 30 nm in diameter. [15, 18] This straightforward setup creates an equilibrium whereby both bound and free Abs exist in the system thereby reducing the overall labeling efficacy of the Ab-AuNP conjugate. The conjugates prepared through this method not only have poor biocompatibility, they also tend to form

nonspecific and promiscuous adsorption to proteins which lead to agglomeration.[18] The complication of biocompatibility of Ab-nanoparticles in biological system remains an obstacle to overcome in order to design an unprecedented probing tool.

In spite of the difficulty and complexity in working with Abs, this quaternary protein structure remains an ideal candidate to work with in engineering a novel Ab-AuNP conjugate. Antibodies, also known as immunoglobulins (Igs) are the antigen receptors produced by B-cells in the immune system. This large protein molecule bears a Y-shape, which is made up of two similar light chains and two similar heavy chains (Figure 1.1). The light chains give the antigen specificity and form the variable region whereas the heavy chains are usually the constant region. Each region consists of a different number of domains, of which each domain contains roughly 110 amino acid units.[19, 20] One significant character of Abs is the hinge region which makes the light chains resemble a flexible arm.[20]

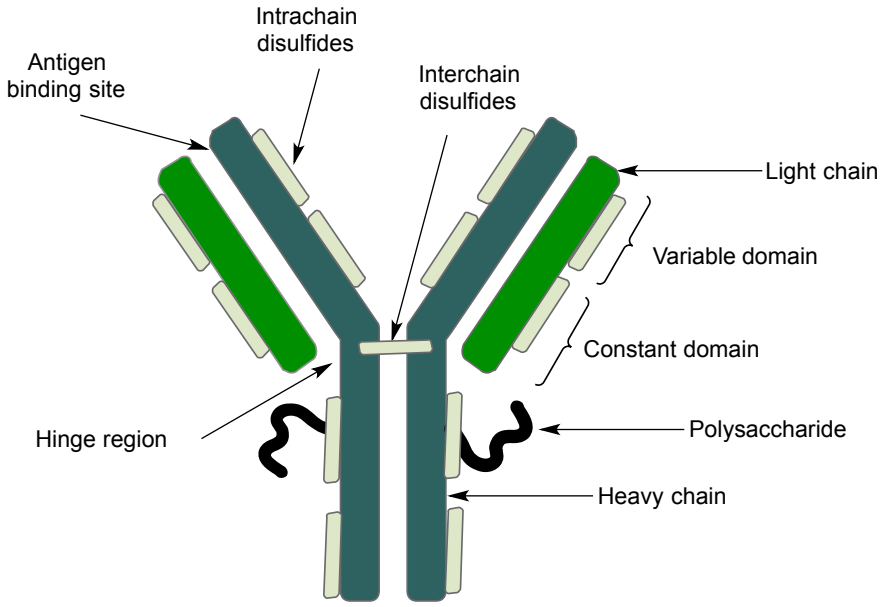

Figure 1.1. Schematic representation of the structure of a monoclonal IgG. Image adapted from ref. 32.

The role played by Abs in the immune system is vital and essential, whereby the effector responses are mediated when the antibody combines with its complementary antigen through non-covalent bonding at the antigen-combining site through a mechanism analogous to the lock and key of enzyme and substrate. The antigen-

combining site of the antibody is found at the variable region and this cleft is specific to the epitope of a particular antigen, which is a small, definitive region recognisable by the immune system. The specificity of the antibody-antigen relationship has sparked several interests and are being intently researched for its use as a nanotool.

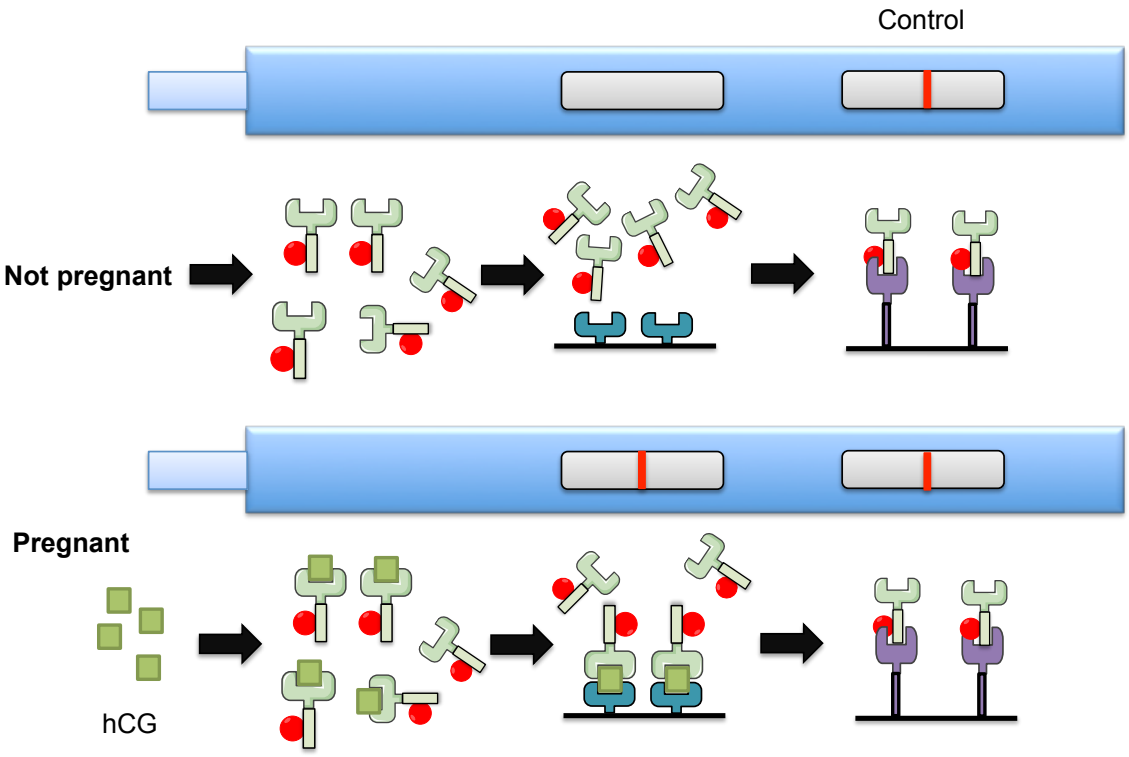

Figure 1.2. Schematic representation of a typical immunoassay of home pregnancy test kit which detects human chorionic gonadotropin (hCG) hormone.

Today, one of the most eminent applications of Ab-AuNP conjugates is their use as probes for biomarkers in pregnancy test kits. The science behind this test is an immunoassay based on the detection of human chorionic gonadotropin (hCG) hormone by AuNP bioconjugated with an anti-hCG antibody (Figure 1.2).[21] Using a similar methodology, AuNP conjugated with an antibody found several other applications in diagnostics such as; immunoassay of antigens from schistosomes and rubella viruses,[22] detection of thrombin (an enzyme responsible in blood clot formation),[23] accurate detection and staging of cancer cells, [18, 24] and determination of markers for Alzheimer's disease.[25] In addition to that, the use of Ab-AuNP conjugates as therapeutic agents are currently being highlighted. For the first time in 2003, AuNPs were used for photothermal therapy, later renamed as plasmonic photothermal therapy (PPTT).[26, 27] This treatment selectively damages the targeted cells, with the AuNP labeled with T-

lymphocytes accumulating at tumour cells before being heated by absorption of laser radiation by the gold particles. Another two Ab-AuNP candidates which have made it farther into the medicinal field are Aurasol®, a therapeutic agent for severe rheumatoid arthritis,[28] and AurImmune™, an AuNP bioconjugated with tumour necrosis factor (TNF) as a targeted antitumour drug.[29 – 31]

1.3.3 Lectin-Functionalised Gold Nanoparticles

Similar to antibodies, lectins are capable of specific interactions with certain carbohydrates. Lectins are ubiquitous glycoproteins with molecular weight ranging from 60 kDa to 100 kDa, found in plants and animals.[58] The specific role of lectins in biological systems are disparate, although have been shown to be involved in the recognition of cell-cell interactions and various other carbohydrate-containing molecules, which consequently result in immune responses.[58, 59] For example, the adhesion of pathogens onto host cells are mediated by protein-carbohydrate interactions conserved by the activity of lectins.[58]

Lectins interact with carbohydrates on cell surfaces through non-covalent and reversible interactions.[48] This highly specific binding is classified to be very weak, with binding affinity about 10^{-3} to 10^{-6} M^{-1}.[48] The specific saccharide-binding property of lectins is significantly induced by its oligomeric structure. Lectins typically possess four important sites; metal binding sites, hydrophobic sites which determine the stability of the protein structure, glycosylation sites and carbohydrate binding sites which define the sugar specificity of lectins.[58] In contrast to the highly specific antigen-antibody interactions, lectin interactions with carbohydrates are not only dictated by the carbohydrate itself, but also the linkage between the carbohydrate, the cell surface and the precise orientation of carbohydrates on the cell surface.[54, 60] As such, the comparable features of lectins to antibodies allow the exploitation of this carbohydrate-binding protein in development of lectin-gold nanoparticle conjugates as another class of biosensor.

1.3.4 Gold Nanoparticle Bioconjugation Strategies

There are currently four methods in preparing gold nanoparticle bioconjugates, of which the strategies are mainly based on: i) physisorption through electrostatic, hydrophobic and Van der Waals interaction (Figure 1.3A),[9, 15, 32] ii) covalent coupling through amine or carboxylate groups (Figure 1.3B),[18, 32 - 34] iii) binding with proteins like protein A (pA) or G (pG) from the bacterial cell wall of *Staphylococcus aureus* (Figure 1.3C),[32] and iv) covalent coupling through the oxidised polysaccharide chains of Abs (Figure 1.3D).[32, 35] The chemistries of these methods are relatively selective, and some provide more controlled loading of protein onto AuNPs than the simple physisorption technique. IgG molecules have several functional groups which can be manipulated for conjugation to nanoparticles, specifically amine groups (N-terminal α-amine and lysine ε-amine) and carboxylate groups (C-terminal end, glutamic acid and aspartic acid residues).[32]

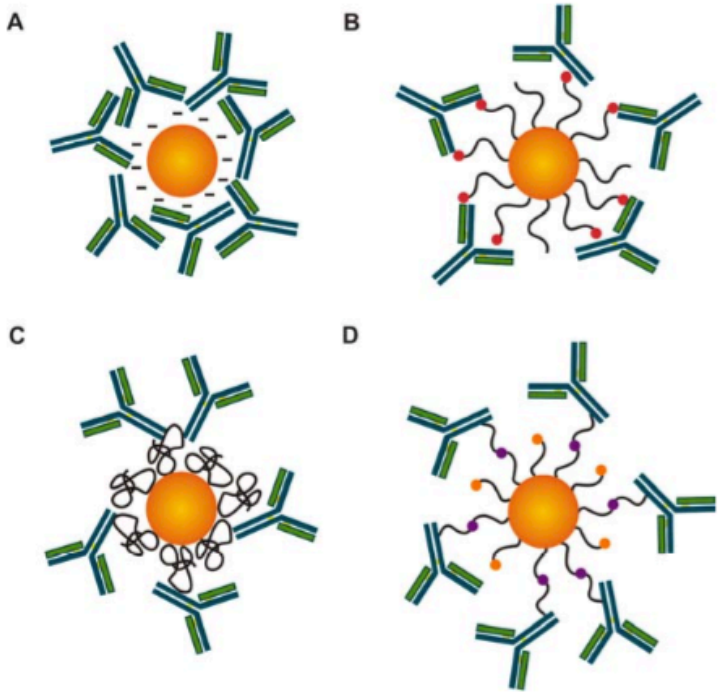

Figure 1.3. Schematic representation of the four strategies in antibody-gold bioconjugation. (A) Adsorption of protein via electrostatic, hydrophobic and Van der Waals interactions. (B) Covalent coupling through activated amine or carboxylate terminal groups. (C) Coupling with proteins (pA or pG) with high binding affinity for the specific fragment crystallisable region (Fc) of the antibody. (D) Covalent coupling through oxidation of oligosaccharide chains of the antibody and functional groups on the particle. Image obtained from ref. 32.

Whilst the strategies discussed above are methods of conjugation typically for antibodies, there are also other examples which employ site-specific conjugation techniques for other types of proteins. One such method is orthogonal bioconjugation which allows a site-specific conjugation of proteins to a nanoparticle as a consequence of mutually reactive electrophilc and nucleophilc pairs.[49] Orthogonal bioconjugation results in conjugation via a pre-selected site without compromising the biological activity of proteins, as such maintaining the three dimensional scaffold of the protein structure. Site-specific conjugation might still be in its infancy stages with several complications to be investigated, but this technique is already being applied to therapeutic nanodevices like aptamer-drug conjugates for targeted drug delivery and cancer therapy. [49, 50]

1.4 Polymer Coating

Despite the approaches addressed, there are still outstanding issues that must be overcome in order to use them efficiently as probes in biological systems. The physicochemical factors, which affect the nanoparticle-cell interactions, remain the main parameter in the architecture of these conjugates. The ideal goal is to prepare a stable and long-circulating nanoparticle in biological medium, for instance in the blood or in tissue samples of living organisms. Many researches have put the spotlight onto the development of probes which could overcome biologically-induced agglomeration and the rapid clearance by the immune system of the body. Ultimately, a rational design of a nanoparticle bioconjugate should demonstrate high selectivity towards the targeted cell receptor and little to no nonspecific binding to other biological components.[36, 37]

The use of a polymer coating on the AuNP before functionalisation with protein is very crucial. One of the popular techniques in achieving better biocompatibility in the conjugates is through the attachment of polyethylene glycol (PEG) on the surface of AuNPs.[38, 39] PEGylated nanoparticles with diameters less than 100 nm have been identified to possess a "stealth" characteristic as they can evade recognition by opsonins and phagocytes in the blood stream thus evading immune system detection.[36] The effective masking of AuNPs by PEG has been established to be due to increased hydrophilicity and reduced nonspecific binding to serum proteins. PEG chains bound to the surfaces of nanoparticles form a boundary described as a "brush" conformation, hence blocking non-specific protein adsorption, improving biocompatibility and thus stabilizing them against agglomeration.

It is also worth noting that the blood circulation half-life of the PEGylated AuNP increases as the molecular weight of the PEG polymer used increases.[36, 40] It is hypothesised that the increased chain flexibility improves the "stealth" characteristic of the nanoparticle, alongside different factors like surface chain density and conformation of coating of the polymer. The high affinity of the gold surface towards thiol (-SH) functional group to form a covalent Au-S bond offers a great amenity for this method of surface modification. Simply, several experiments were conducted by attaching thiolated PEG onto the surface of AuNPs.[18, 34 – 40]

1.5 Aims and Objectives

Considering the subjects discussed above, this work aims to develop a strategy to attach different types of protein including carbohydrate-binding proteins called lectins and antibodies onto polymer coated AuNPs. Essentially these bioconjugates could be used as sophisticated biosensors which could detect protein-protein interactions in biological systems.

This report intends to explore a versatile but facile method for protein conjugation onto gold nanoparticles, employing the 1-ethyl-3-(3-dimethylaminopropyl) carbodiimide hydrochloride/*N*-hydroxysuccinimide (EDC/NHS) activation chemistry. Several factors in this conjugation technique will be explored and optimized in order to achieve a highly efficient method. The protein activities in the resulting bioconjugates should be retained and this should be confirmed by testing through carbohydrate binding assays and immunoassays.

2. Results and Discussion

2.1 PEGylation of Gold Nanoparticles

Colloidal gold with a diameter size of 40 nm is used in this report. This size has been chosen particularly for its red colouration which allows quick detection of aggregation due to visible colour change whilst retaining the small size needed for a biosensor. Due to the high affinity of thiol group towards gold metal, PEG-2-mercaptoethyl ether acetic acid (Figure 2.1), a bifunctional polymer structure with an average molecular number, M_n of 3500 was used as a stabilising agent to prevent the particles from aggregating. The sulfur end of the PEG chain would conjugate to gold via a sulfur-gold bond, allowing the activation of carboxylic acid end via EDC/NHS coupling in the next step.

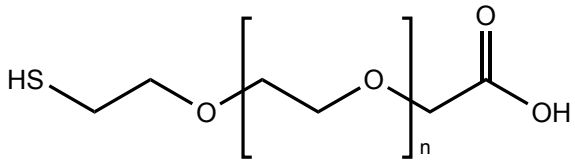

Figure 2.1. Chemical structure of PEG-2-mercaptoethyl ether acetic acid. The thiol end is attached to surface of AuNP whilst the carboxylate end remains as an active functional group for conjugation.

The prepared colloidal PEG-AuNP was characterised using UV/Vis spectroscopy. TEM characterisation was omitted since the gold colloid used were purchased and have been characterised by the manufacturer. The absorption maximum of the measured UV/Vis spectra of the colloidal solution provides information on the average size of AuNP. The UV/Vis spectra of AuNP and PEG-AuNP display an absorption maximum at 525 nm and 527 nm respectively. The values of the absorption maximum represents the SPR absorbance of the nanoparticle, whilst the 2 nm shift of the SPR maximum indicates an increase in size of the nanoparticle. This was expected as conjugation of PEG chain onto AuNP would increase particle size. This has been corroborated by dynamic light scattering (DLS) data (Figure 2.2, Table 2.1). The values of the SPR maximum remain the same during several months, indicating the high stability of both AuNP species.

It is worth noting that these UV/Vis measurements assume that the nanoparticles are spherical in shape, as were the gold colloids used. However, the polymer coating onto AuNPs are expected to be amorphous and indefinite.[51] The maximum absorbance measured is also reliant on the concentration of particles in solution, which decreases with each washing step.

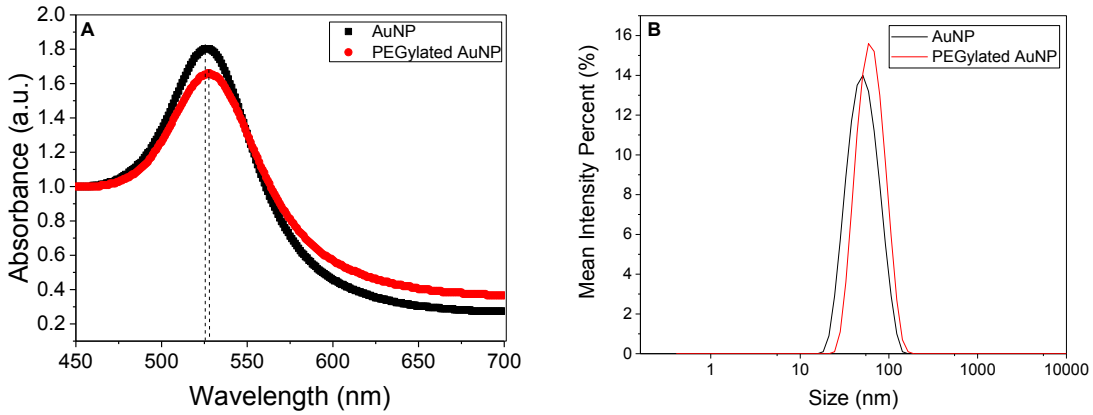

Figure 2.2. (A) Overlaid UV/Vis spectra of AuNP and PEG-AuNP. The SPR peak of PEGylated AuNP sees a slight shift to the right as compared to that of AuNP. (B) Comparison of hydrodynamic diameter of both particles as measured by DLS.

AuNP	Hydrodynamic diameter, d (nm)	Maximum absorbance (a.u.)	Wavelength (nm)
Unfunctionalised	44.8 ± 0.4	1.80	525
PEG-AuNP	55.4 ± 0.1	1.66	527

Table 2.1. Summary table of DLS and UV/Vis spectroscopy data for AuNP and PEG-AuNP.

To confirm the effects of PEG chain on AuNP, the stability of PEG-AuNP conjugate was tested in saline by incubation of conjugates with NaCl solution and PBS in a serial dilution from 1 M and 10 mM respectively. The two AuNP species were incubated with the saline solutions and an obvious contrast in the stability between the PEG-coated AuNP and that of which was not coated could be seen. The unfunctionalised particles were only stable from 20 mM to 60 mM in NaCl and 0.15 mM to 2.50 mM in PBS whilst the PEGylated AuNPs remain stable throughout in all

concentrations tested (Figure 2.3). The visible colour change allows a quick diagnosis of the colloidal stability and this has been corroborated by the UV/Vis spectra measured for both NaCl solution and PBS buffer (Figure S6 and S7, respectively in Supplementary Information).

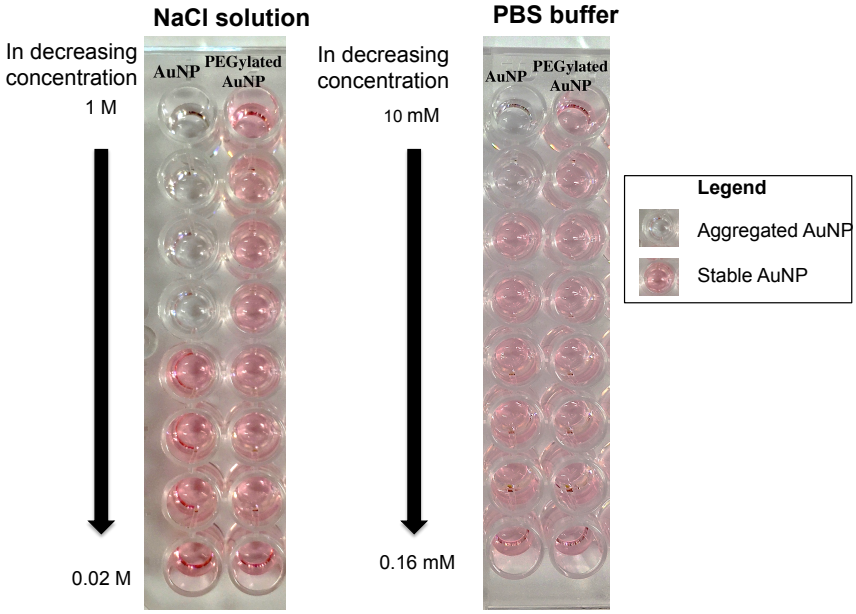

Figure 2.3. Effects of decreasing salt concentration on the stability of AuNP and PEG-AuNP. The images show sections of 96-well plates containing nanoparticles in NaCl solutions and PBS buffer after incubation at room temperature (RT) for 30 min.

2.2 Preparation of Protein-Gold Conjugates

EDC/NHS activation chemistry was employed due to its versatility, providing a convenient method for conjugation of proteins onto the surface of nanoparticles. EDC binds initially to the carboxylate group on the surface of functionalised AuNPs forming an *O*-acylisourea intermediate.[52] NHS is used to stabilise the intermediate in this crosslinking reaction, forming a semi-stable amine-reactive NHS ester, which can easily be replaced by an amine functional group (Figure 2.4). There are several factors governing the efficiency of this activation reaction, which includes the ratio of EDC/NHS used and pH of reaction media. A ratio of EDC/NHS of 1:1.5 was used in this reaction, with a fresh solution prepared for one activation round. This activation process was carried out in pH 5.0 using MES buffer which is a compatible reaction buffer for carbodiimide.

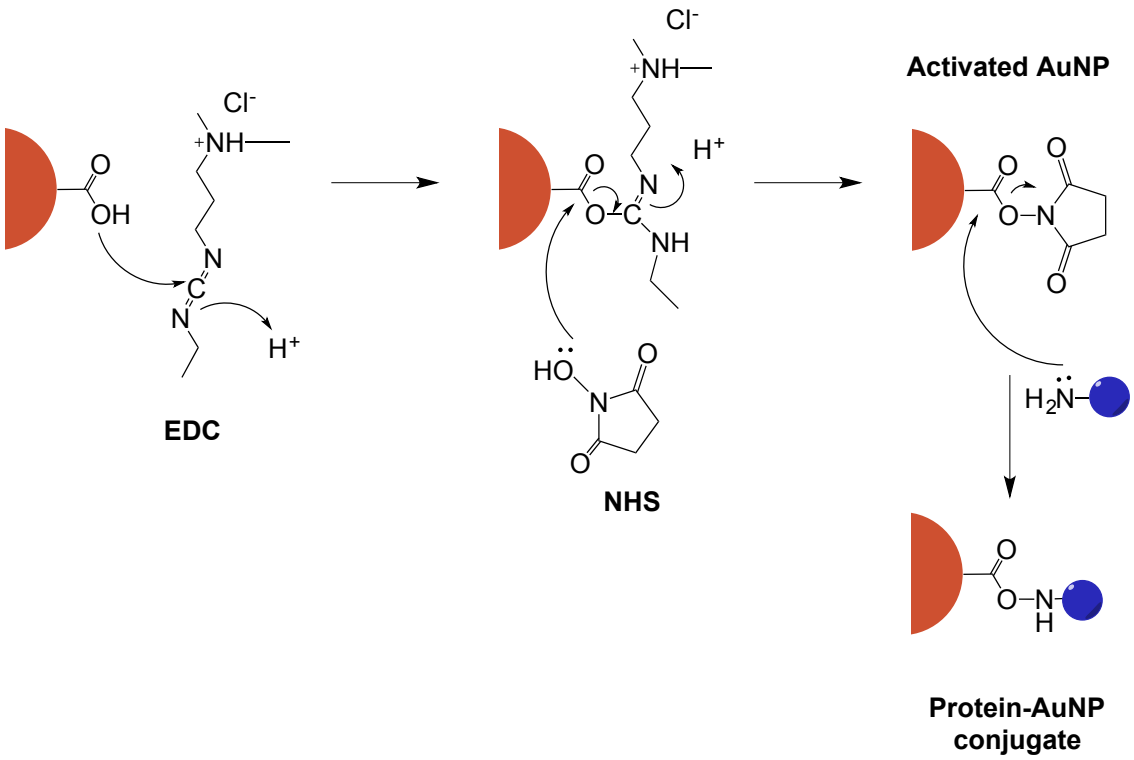

Figure 2.4. Reaction scheme of EDC/NHS activation for carboxyl-to-amine crosslinking. Addition of NHS to EDC reactions not only increases efficiency of reaction but also enables the storage of activated nanoparticle for future use.

The semi-stable amine-reactive NHS ester (the term "activated AuNP" is sometimes used to describe this structure) was characterised using UV/Vis spectroscopy, recording a SPR peak at 530 nm. The shift in the SPR maximum shown

by the activated AuNP species is due to the increased hydrophobicity of the structure as an effect of addition of hydrophobic NHS ester, instead of the increase in polymer size as was discussed before. The broader distribution represents a greater dispersity in polymer size and also a possibility of aggregation of AuNPs, since the NHS ester structure is only partly stable. The DLS data is in agreement with that obtained from the UV/Vis measurements (Figure 2.5), with several peaks seen in the DLS measurement of the activated AuNP species due to formation of aggregates, which then break up as protein displaces the coupling reagent (Figure 2.6). This reactive intermediate is extremely hygroscopic as water can hydrolyse the ester structure to form a carboxylic acid functional group again.

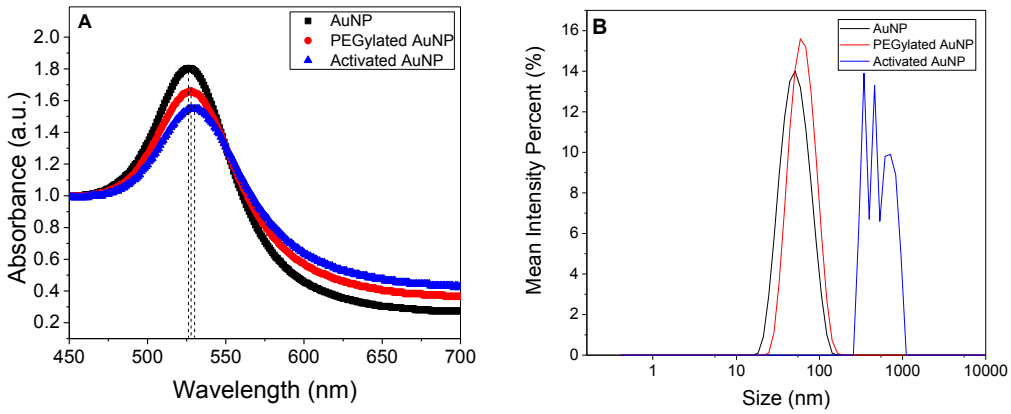

Figure 2.5. (A) Overlaid UV/Vis spectra of AuNP, PEGylated AuNP and activated AuNP. The blue/red shifts seen between the three species confirm the change in nature of the nanoparticles following each reaction step. (B) Size distribution by intensity of the three AuNP species as measured by DLS.

Activated AuNPs were washed to remove the isourea by-product and excess activating agent which may compete with the protein structure for conjugation. These reactive structures were then incubated with proteins dissolved in PBS (pH 7.4) at RT for 4 h. Lysine residues are the primary target for EDC/NHS conjugation due to the primary amine R-group. Conjugation with different proteins; albumin from bovine serum (BSA), peanut agglutinin from *Arachis hypogea* (PNA), *Dolichos biflorus* agglutinin (DBA) and Concanavalin A (Con A), form protein-gold conjugates, linked by an amide bond which is stable. The orientation of lectins onto AuNPs during conjugation was disregarded due to the oligomeric structure of lectins which form several carbohydrate binding sites.

The conjugation was confirmed via characterisation of conjugates by UV/Vis spectroscopy and DLS measurements (Figure 2.6, Table 2.2). The SPR peaks of the protein-AuNP conjugates see a slight blue shift, which was unexpected as the particles are conjugated to a large protein structure. However, this shift could be due to the folding of protein structure when coupled to the particle, which results in a smaller effective size than the activated AuNP.

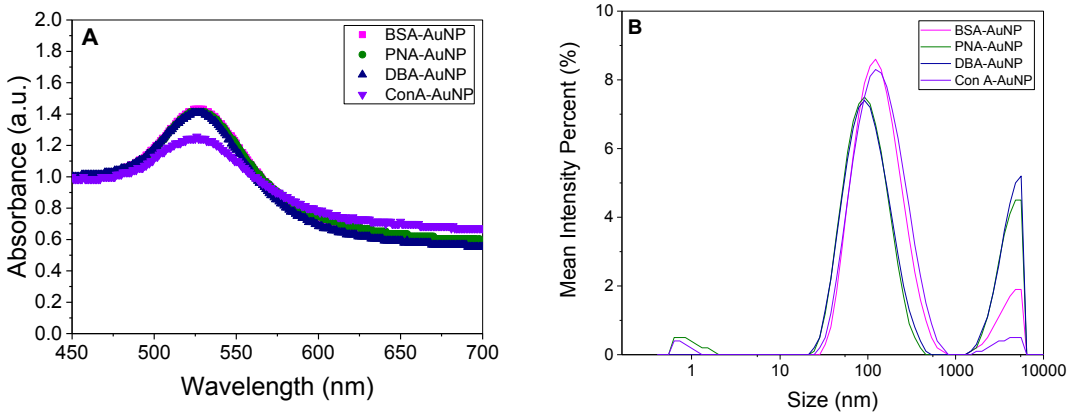

Figure 2.6. (A) Overlaid UV/Vis spectra of the four different protein-AuNP conjugates. (B) Size distribution by intensity of the four different protein-AuNP conjugates as measured by DLS. The peaks at the right are due to aggregated AuNPs or large dust particles.

AuNP	Hydrodynamic diameter, d (nm)	Maximum absorbance (a.u.)	Wavelength (nm)
BSA-AuNP	134 ± 17	1.43	527
PNA-AuNP	180 ± 46	1.41	527
DBA-AuNP	196 ± 55	1.41	527
Con A-AuNP	114 ± 4	1.26	526

Table 2.2. Summary table of DLS and UV/Vis spectroscopy data for protein-AuNP conjugates. There is high error in DLS measurements due to aggregation of AuNP.

Infrared (IR) spectroscopy was also employed to confirm the conjugation of protein onto activated AuNP. The IR spectra of BSA-AuNP was compared against that of

PEGylated AuNP, and slight shifts in the absorption peaks were observed, proving that formation of protein-AuNP was successful (Figure 2.7A, Table 2.3). The IR spectra of PEGylated AuNP and a mixture of PEGylated AuNP with solution of BSA incubated without EDC/NHS activation as a control was also compared (Figure 2.7B). The peaks of both spectra are similar, indicating that activation of AuNP is essential for conjugation.

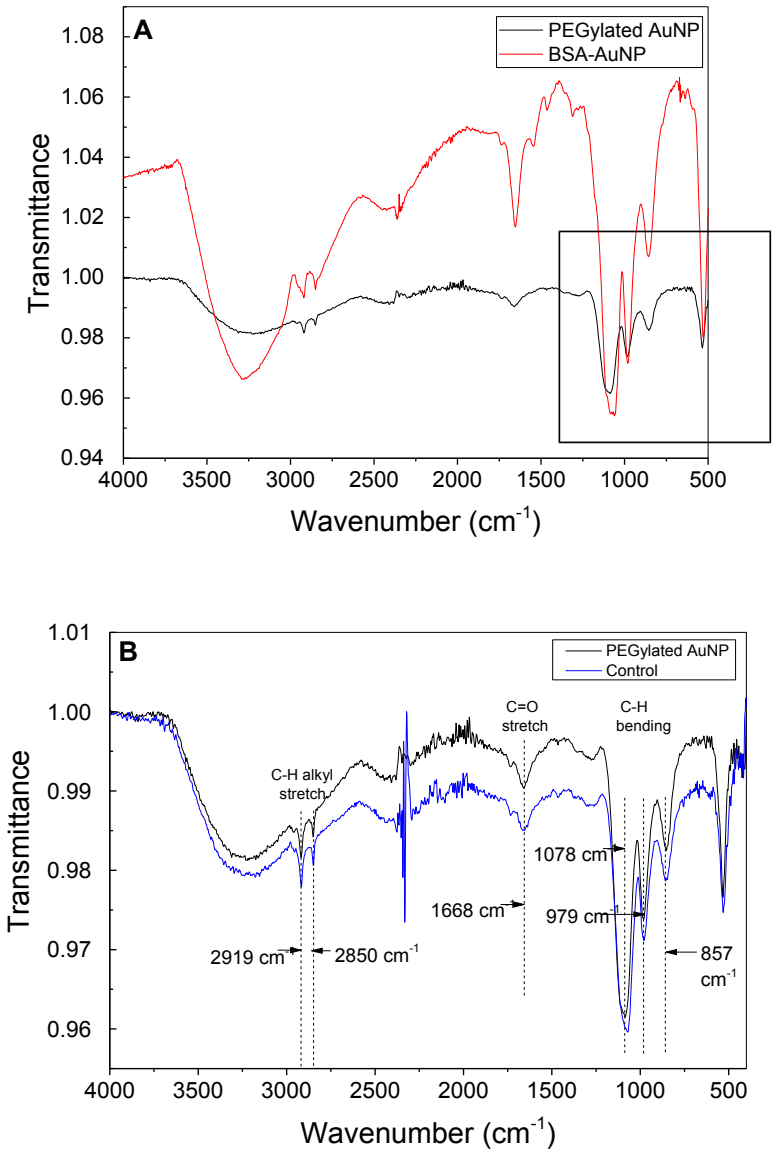

Figure 2.7. (A) Overlaid IR spectra of PEGylated AuNP and BSA-AuNP conjugate. (B) IR spectra of PEGylated AuNP and mixture of non-activated PEGylated AuNP with BSA as control.

AuNP	Wavenumber (cm^{-1})					
	C-H alkyl stretch		C=O stretch	C-H bending		
PEGylated AuNP	2919	2850	1668	1078	979	857
BSA-AuNP	2910	2840	1653	1060	980	857

Table 2.3. Shifts in wavenumbers as seen in Figure 2.7A between PEGylated AuNP and BSA-AuNP which indicates successful conjugation of protein onto activated AuNP.

The characterised IR spectra of all protein-AuNP conjugate species can be found in Supplementary Information.

2.3 Kinetic Study on Conjugation of Proteins to Gold Nanoparticle

Several optimisation of the conjugation steps discussed above were carried out in order to determine the most efficient strategy. Buffers and salt compatibility play an important role in maintaining particle stability. In this report, the activation buffer used was 100 mM MES buffer (pH 5.0) and the coupling buffer used was 10 mM PBS (pH 7.4). This pH range is optimal for the reactivity of NHS ester.[57]

Another key criterion in the conjugation of proteins onto activated AuNPs is the conjugation time. The optimal conjugation time varies between different protein types due to different stability of the protein structures.[57] As such, the optimal conjugation time for lectins are tested by performing a kinetic study on conjugation time versus final result output for the molecules conjugated. Mannan is a polysaccharide of repeating mannose units and Con A binds to mannose. Hence, through binding to mannan, aggregation of the particles would be achieved. Here, Con A was conjugated to AuNP for 1 h, 2 h, 3 h, 4 h and overnight, then tested in a mannan binding assay performance (Figure 2.8).

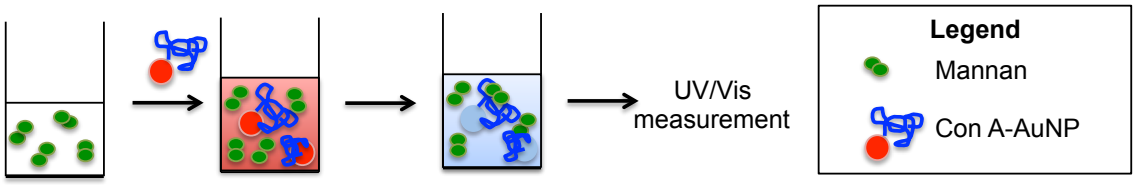

Figure 2.8. Mannan binding assay to test performance of Con A-AuNP conjugated for different times. The assay was carried out in 10 mM HEPES buffer containing 0.05 M NaCl, 0.1 mM $CaCl_2$ and 0.01 mM $MnCl_2$ due to the salt dependence binding of sugar to Con A.[53]

The binding assay was tested in solution phase and a qualitative visible colour change can be detected alongside a more quantitative results from UV/Vis measurement. The effects of conjugation time on the performance of mannan-binding assay were obvious. The absorbance maxima decreases as conjugation time increases from t = 0 to 4 h. When left overnight, the UV/Vis spectra returned to give a response comparable to PEGylated AuNP (Figure 2.9). A broad peak of the UV/Vis spectra denotes a great degree of aggregation of AuNPs due to binding with mannan.

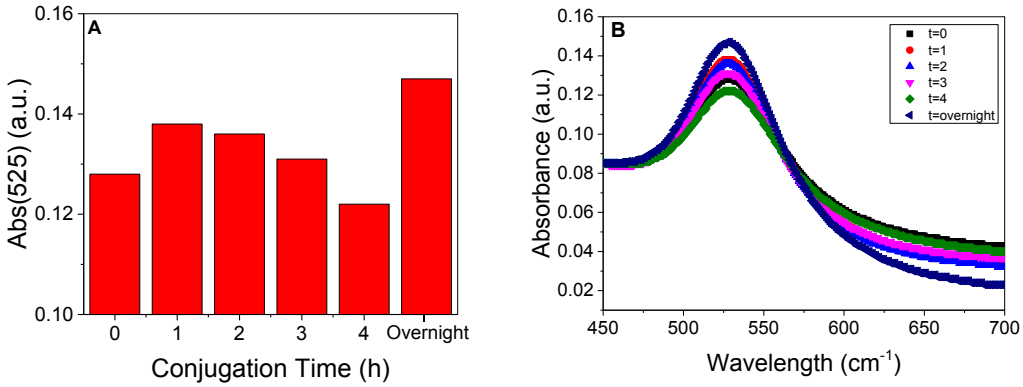

Figure 2.9. (A) Bar chart showing the absorbance value at 525 nm for different conjugation times. (B) UV/Vis spectra of Con A-AuNP conjugated for different times incubated in mannan solution.

Activated AuNPs incubated with Con A for 4 h shows the best results. This was confirmed with apparent visible colour change from red to blue then colourless in the 384-well plate which were not detected in other conjugation times. A longer conjugation time leads to increased conjugation of protein structure onto surface of activated AuNP, and this was attributed as the reaction time of the conjugation process.[64] As such it could be said that the number of Con A conjugated onto activated AuNP increases over time, up to 4 h, leading to greater aggregation signal in mannan solution as shown in Figure 2.9. Conjugation time of more than 24 h as suggested by Mason *et al*.[18] was not optimum utilising this protein. From the UV/Vis spectra, it could be hypothesised that the conjugation time of more than 24 h led to the denaturation of protein structure or aggregation of the particles as the conjugates clump together, leading to poor and little response in the mannan binding assay.

2.4 Carbohydrate Binding Assays

Four different proteins, namely BSA, PNA, DBA and Con A were used to form the protein-AuNP conjugates. Covalent bioconjugation can affect the function and activity of the proteins, which results in protein denaturation. Therefore it is important to test the activity of the conjugates produced. The lectins have different sugar specificity hence sugar binding assays using different monosaccharides, specifically galactose, glucose and mannose were carried out to test the efficacy of the conjugates, whilst non-specific adsorption was tested using BSA (Table 2.4).

Lectins	Abbreviation	Sugar Specificity
Peanut agglutinin	PNA	Galactose
Dolichos biflorus agglutinin	DBA	*N*-Acetylgalactosamine (GalNAc)
Concanavalin A	Con A	Glucose/Mannose

Table 2.4. Sugar specificity of the lectins and their abbreviations as extracted from ref. 56.

These assays were carried out using surface-bounded sugar moieties, where 96-well plates with hydrazide functionality were used to couple monosaccharides using aniline as catalyst at 50 ˚C and incubation for 24 h to form glycosylated surfaces (Figure 2.10A). Coupling of monosaccharides via this mechanism is known to result in attachment primarily in the ring closed β-anomeric form.[55] The glycosylated surfaces were then analysed by modified drop shape analysis, of which the droplet spread was measured. When viewed from above, a hydrophobic surface gives reduced surface coverage as compared to hydrophilic surface at equal volume. The hydrazide surfaces resulted in only 10% coverage by the droplet, as compared to the sugar functionalised surfaces, with over 15% coverage (Figure 2.10B).

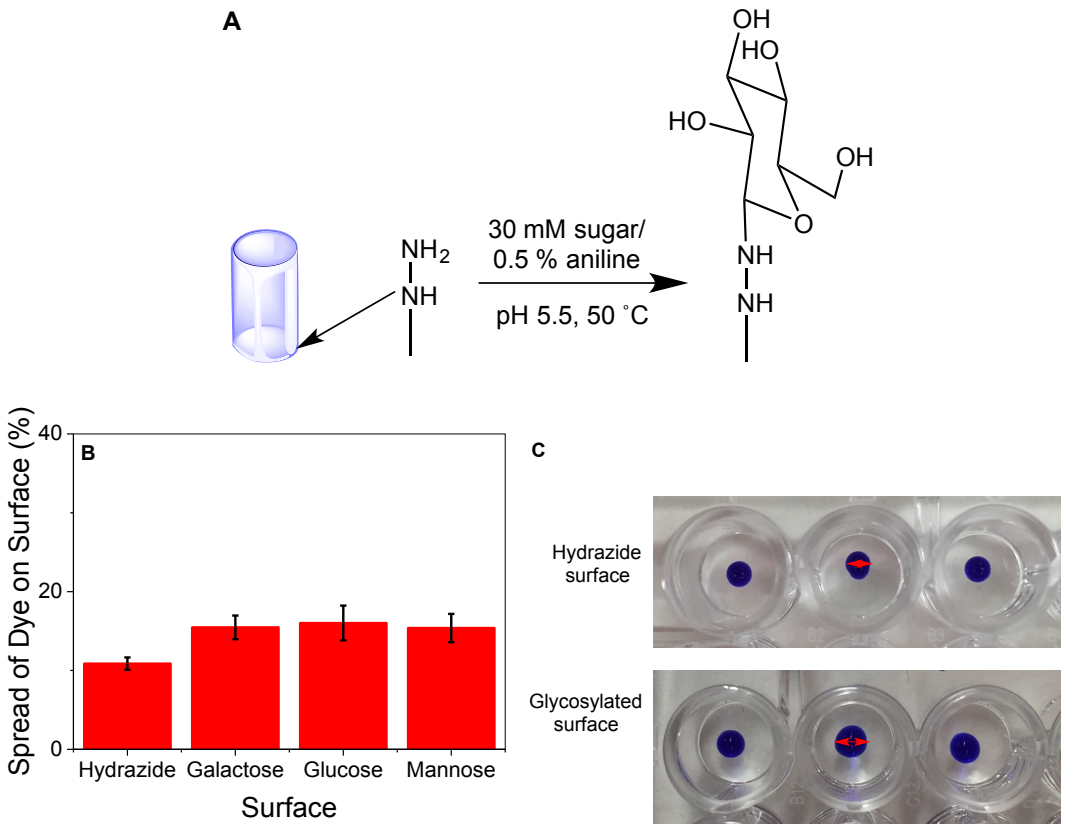

Figure 2.10. (A) Glycosylation of 96-well plates via hydrazide-carbohydrate coupling. Image adapted from ref. 54. (B) Relative hydrophilicity of surfaces as measured by dye spreading assay. (C) Snapshot of the spread of dye on hydrazide and glycosylated (mannose) surfaces.

The monosaccharide binding assays were carried out via exposure of varying concentrations of protein-AuNP conjugates onto the sugar surfaces (Figure 2.11). After which, the surfaces were washed and the UV/Vis absorbance from 450 to 700 nm were measured. This assay fundamentally depends on UV/Vis spectroscopy to detect the presence of gold bioconjugates in the 96-well plates. As a negative control, PEGylated AuNP were incubated with each surface and as expected, the SPR peak is absent from the UV/Vis spectra. Conclusively, PEGylated AuNP do not bind to the carbohydrate surfaces and lectins conjugated to colloidal gold are responsible for the binding activities.

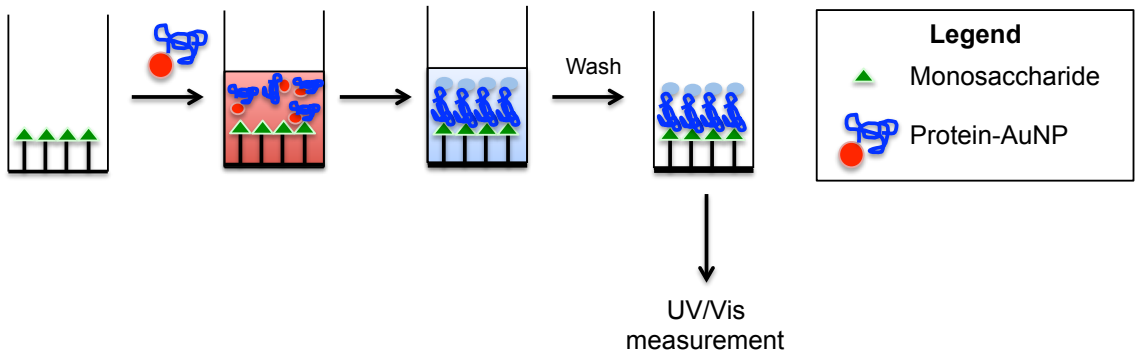

Figure 2.11. Carbohydrate binding assay to test the efficacy of different protein-AuNP conjugates.

For different glycosylated surfaces, the attachment of protein-AuNP conjugates varies due to different sugar binding specificity of lectins. From the UV/Vis spectra obtained, the absorbance value at 525 nm of each conjugated species when 60 μg.mL^{-1} gold colloid was added were normalised and compared against one another (Figure 2.12). The presence of a peak in the UV/Vis spectra (Figure S8, S9 and S10 in Supplementary Information) denotes the presence of conjugated AuNP species in the wells. The proportional relationship between the intensity of the absorbance measured and the concentration of the lectin-AuNP also proves that binding on the sugar surfaces occurred.

The values for both PEGylated AuNP and BSA-AuNP in all three surfaces are comparable, which represent some non-specific to no binding on the sugar surfaces. The relatively high values recorded by PNA-AuNP conjugates on every surface signify random and promiscuous binding behavior, which is a typical character of PNA. Even though PNA is customarily recognised to be β-galactose specific, microarray analysis has shown that this lectin readily binds all monosaccharides with little difference between them.[54] As such, the results recorded by PNA-AuNP conjugates were omitted from analysis.

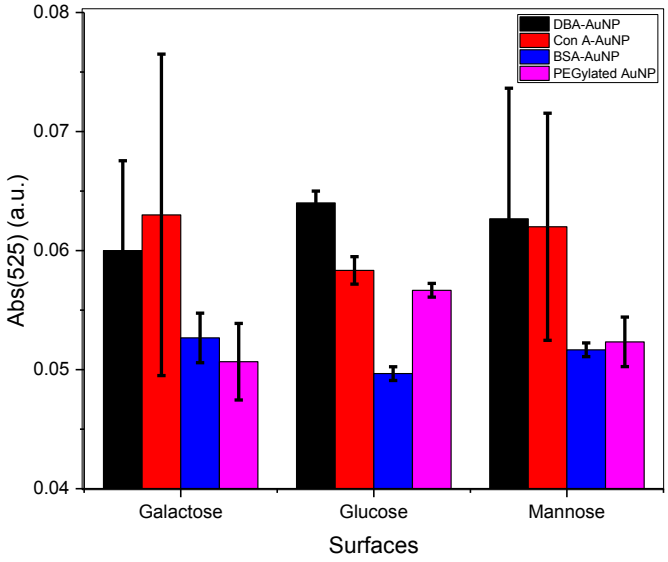

Figure 2.12. Comparison of absorbance maxima values for various lectin-gold bioconjugates (60 μg.mL^{-1} gold colloid, 0.3 μmol of gold) in carbohydrate binding assays, where the values are an average of three repeats and the errors represent the standard deviation.

From the results shown in Figure 2.12, Con A-AuNP shows binding to both glucose and mannose surfaces, consistent with its class as a mannose/glucose binding lectin. The higher absorbance value on mannose surface compared to that of glucose also reflects the greater affinity of Con A for sub-terminal and terminal mannose and weaker affinity for terminal glucose.[60, 61] DBA, a *N*-acetyl-D-galactosamine (GalNAc) specific lectin also shows indifferent binding to oligosaccharides with terminal galactose.[62] Hence, binding activities were detected by DBA-AuNP conjugates on galactose surfaces as seen in Figure 2.12. Overall, the binding activities of both Con A and DBA conjugates were comparable, with minor carbohydrate specificity between them. This could relate to the fine specificities between lectin-carbohydrate interactions, which still require more understanding. However, apparent binding of the lectin-AuNP conjugates to the carbohydrate surfaces proved the efficacy and retainment of activity of proteins after conjugation.

The binding of protein-AuNP conjugates onto sugar surfaces was also confirmed using modified drop shape analysis (Table 2.5). The increase in the percentage of dye spread on the surfaces incubated with the protein-AuNP conjugates as compared to that

with sugar functionalisation proved that the hydrophilicity of the surfaces have changed. Surfaces treated with BSA-AuNP showed the greatest change, recording a percentage dye spread above 20 % and this could possibly be due to non-specific binding of protein onto the surfaces. Surfaces treated with normal PEGylated AuNPs as negative control shows a percentage spread of dye within the range comparable to the untreated surfaces, once again affirming no binding activities from PEGylated AuNP species.

The values for the surfaces treated with PNA-AuNP, DBA-AuNP, Con A-AuNP show only slight difference from that of the untreated sugar surfaces, some with large errors. This is possible as a protein structure is made of several regions, including hydrophobic and hydrophilic regions. Different exposure of the regions to the dye could affect the spread of dye on surface. Hence, although the true binding behaviour of the conjugates cannot be verified, it could be confirmed that treatment of sugar surfaces with protein-AuNP conjugates does affect the characteristic of the surfaces, implying that protein is bound to AuNPs.

Surface	Galactose	Glucose	Mannose
Untreated	15.5 ± 1.5	16.0 ± 2.2	15.4 ± 1.8
PEGylated AuNP	16.5 ± 2.1	15.8 ± 0.6	16.8 ± 0.4
BSA-AuNP	22.1 ± 1.1	21.5 ± 4.2	21.9 ± 0.6
PNA-AuNP	23.2 ± 2.7	16.4 ± 0.5	21.9 ± 6.3
DBA-AuNP	17.5 ± 2.3	16.8 ± 2.3	20.2 ± 2.7
Con A-AuNP	20.6 ± 5.0	16.0 ± 2.0	18.2 ± 5.1

Table 2.5. Percentage spread of dye on different sugar surfaces treated with various protein-AuNP conjugates, where the values are an average of three repeats and the errors represent the standard deviation.

2.5 Anti-IgG Binding Assay

As proven to work by the protein-AuNP conjugates on glycosylated surfaces and in mannan solution, the optimised conjugation conditions were applied to prepare Ab-AuNP conjugates (the term IgG-AuNP is also used interchangeably). The conjugate was characterised using UV/Vis spectroscopy, DLS measurements and IR spectroscopy to confirm the conjugation. The blue shift in the activated AuNP species upon addition of IgG confirms the conjugation of antibody to form a stable particle, with a SPR peak at 527 nm (Figure 2.13A). The hydrodynamic diameter as measured by DLS is 350 ± 70 nm, which is significantly larger than the PEGylated AuNP (Figure 2.13B). This could be due to the adsorption of antibodies between two or more AuNPs hence forming large aggregates (Figure 2.14).[32, 63] This is a typical problem in formation of Ab-AuNPs. The formation of aggregates was further confirmed by DLS from which an increase of size (> 700 nm) was measured after the conjugates were left overnight.

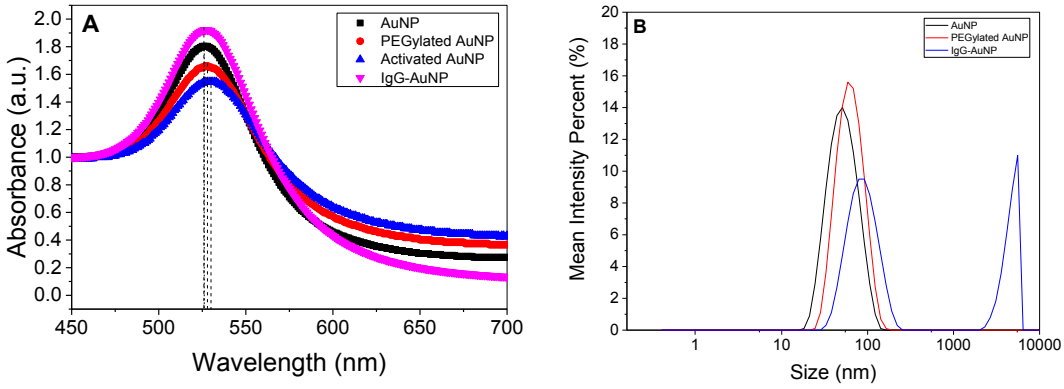

Figure 2.13. (A) Overlaid UV/Vis spectra of the four different AuNP species during the preparation of IgG-AuNP. (B) Size distribution by intensity of 40 nm AuNP, PEGylated AuNP and IgG-AuNP as measured by DLS. The peak at the right is largely due to aggregated AuNPs.

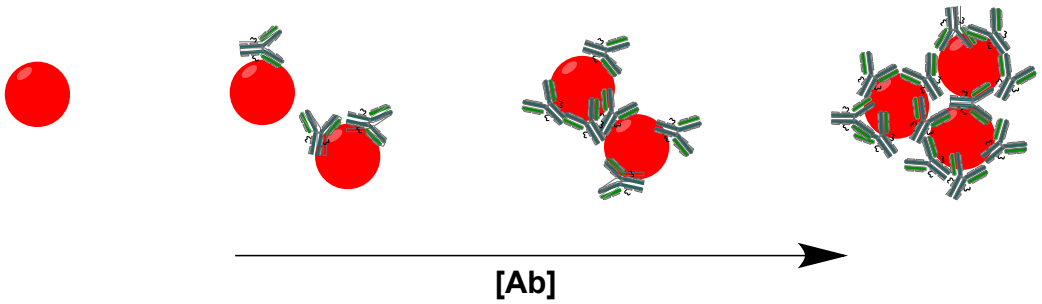

Figure 2.14. Schematic diagram of IgG-AuNP bioconjugate configuration as a function of number of antibody molecules bound onto the AuNPs, leading to the formation of large aggregates. Image adapted form ref. 32.

These conjugates were tested on anti-IgG binding assays to determine their efficacy and efficiency. The assays were performed in triplicates to avoid errors and negative controls were in the form of PEGylated AuNP. Standard solutions with known concentrations of IgG from rabbit serum were prepared to obtain a standard curve (Figure 2.15A, Table 2.6). The IgG concentration in the conjugate sample was determined by interpolation between points on the curve. The 60 μg.mL^{-1} gold conjugate sample yielded an average absorbance reading of (0.897 ± 0.06) a.u., a signal significantly lower compared to the negative control (Figure 2.15B). These results demonstrate antigen-antibody binding activities in the IgG-AuNP sample, but not in the PEGylated AuNP sample, affirming the successful conjugation of antibody onto surface of AuNP.

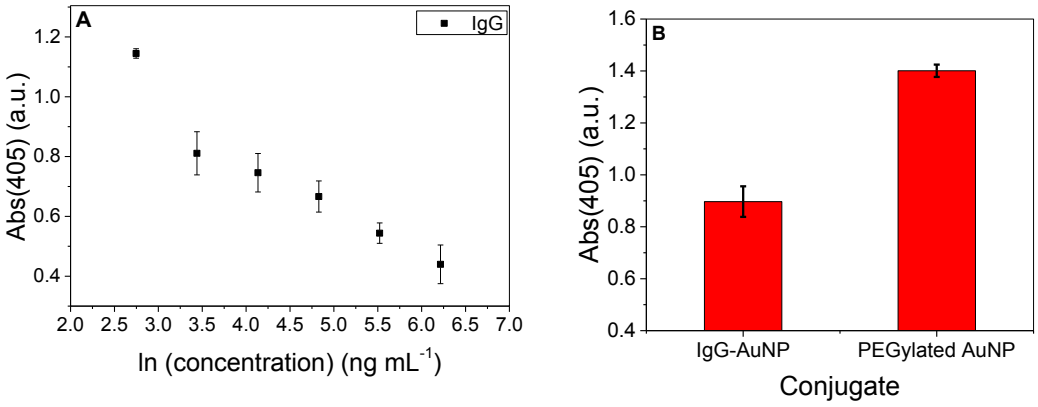

Figure 2.15. (A) Absorbance value at 405 nm against ln(concentration) of IgG. IgG samples were used as a positive control whilst PEGylated AuNP acts as a negative control. (B) Bar chart showing absorbance values at 405 nm of IgG-AuNP and PEGylated AuNP (concentration 60 μg.mL^{-1} of gold), where the values are an average of three repeats and the error represents the standard deviation.

Concentration of standard ($ng.mL^{-1}$)	ln(concentration) ($ng.mL^{-1}$)	Absorbance (405 nm) (a.u.)
500.0	6.21	0.440 ± 0.06
250.0	6.21	0.544 ± 0.03
125.0	4.83	0.666 ± 0.05
62.5	4.14	0.746 ± 0.06
31.2	3.44	0.811 ± 0.07
15.6	2.75	1.145 ± 0.02

Table 2.6. Anti-IgG assay standard curve values, where the values are an average of three repeats and the error represents the standard deviation.

$$Concentration\ of\ IgG\ in\ sample = C_1 + C_1\frac{(Abs_1 - Abs_{sample})}{(Abs_1 - Abs_2)}$$
$$= 15.6 + 15.6\frac{(1.145 - 0.897)}{(1.145 - 0.811)}$$
$$= (27.2 \pm 0.2)\ ng.mL^{-1}$$

Equation 1. Linear interpolation equation where C_1 is the concentration of IgG of the lower boundary, C_2 is the concentration of IgG of the upper boundary, Abs_1 is the absorbance value corresponding to C_1, Abs_2 is the absorbance value corresponding to C_2 and Abs_{sample} is the absorbance value of the sample.

The linear interpolation equation (Equation 1) was used to calculate the concentration of IgG in the sample. This anti-IgG assay is the easiest and fastest way of determining the loading of Ab onto AuNP, whilst maintaining a degree of precision. Other methods which could help determine the loading density of Ab onto AuNP are x-ray photoelectron spectroscopy analysis (XPS) and thermogravimetric analysis (TGA), but these methods are time consuming. The concentration of IgG in the conjugate was found to be (27.2 ± 0.2) $ng.mL^{-1}$ in every 60 $\mu g.mL^{-1}$ of gold colloid. Based on this calculated value, the mass of antibody is found to be 0.05 % of the gold particle. This value is considerably low if compared to works by other groups.[34, 63] This difference could

be possibly induced by the high degree of aggregation of the conjugates synthesised, resulting in a lower average number of effective antibody bound per AuNP. As such it is vital to determine several factors in order to find a satisfactory compromise between formation of rightly conjugated particles and large aggregates. These include the optimal concentration of IgG solution used in incubation and optimal conjugation time when preparing the bioconjugate.

One key question to address is the bioactivity of Ab-AuNP as compared to unbound antibody molecule. Referring to the low density loading of antibody onto AuNP as calculated, a hypothesis that the bioactivity of this conjugate is lower compared to that of the primary response of the antibody was suggested. A recent work by van der Heide and Russell[63] has elucidated this hypothesis, of which the IgG-AuNP synthesized via attachment by activated carboxylate terminal group yielded a lower activity signal as compared to free antibody itself. This is due to the exclusion of the orientation of the antibody structure upon coupling. Binding of antibody through EDC/NHS activation of carboxylate terminal group is random, via one of the several amine groups present in the antibody structure. This results in the reduced exposure of antigen-binding (Fab) region and subsequently less binding ability, therefore producing a weaker detection signal.

3. Conclusion and Future Works

A relatively simple, economical and scalable covalent bioconjugation method has been tested and optimised to prepare protein-AuNP conjugates. Over a period of time, a lot of effort has been put into finding the most efficient way to covalently load biomolecules onto AuNPs for the purpose of applications as biosensors. A series of bioconjugates made of lectins and monoclonal IgG that can be used in specific recognition of carbohydrates and antigens through molecular interactions were prepared and tested in both solution and solid (surface) phases. It is a promising discovery to know that such a simple conjugation technique could produce a workable and practical nanotool.

3.1 Preparation of Lectin-AuNP Conjugates

The protein-AuNP conjugates were prepared through a refined method manipulating EDC/NHS activation chemistries. Whilst this method is simple and straight forward, it is important to realise several factors including; the ratio of EDC to NHS used, pH of the buffer solution and presence of water in the reaction medium, as these could affect the efficiency of the reaction. An efficient activation process could lead to a more efficient loading of protein onto particles, hence high precision of methodology plays an important role in the preparation of bioconjugates. The preparation of PEGylated AuNP and activated AuNP can be confirmed by simple characterisation methods like UV/Vis measurements, alongside corroboration by DLS data. Another essential point to note is the optimal conjugation time of proteins with activated AuNP. Different protein structures have different conjugation time due to their varying stability at RT and different reaction media. From this investigation, an optimal conjugation period of 4 h has been chosen and applied generally onto all methods. This conjugation period has proved to be optimal as all four protein-AuNP conjugates were successfully characterised by UV/Vis spectroscopy, DLS measurements and IR spectroscopy.

From the sugar binding assays and surface functionalisation analysis, relevant binding of conjugates onto the surfaces were detected proving the positive results of the conjugates as a simple biosensor. Although the specificity of the binding varies slightly,

especially for DBA-AuNP and Con A-AuNP conjugates, these could be compensated by the large errors which were largely contributed by assay drifts. The experiments could be repeated to obtained results with greater precision and accuracy.

3.2 Preparation of Ab-AuNP Conjugates

As the preparation of protein-AuNP conjugates shows positive results, a similar methodology was applied in preparing monoclonal IgG-AuNP conjugates. Using the simple strategy as tested before, the conjugates were prepared and were successfully characterised by UV/Vis spectroscopy, DLS measurements and IR spectroscopy. The bioactivity of the conjugates were found to be lower than free antibody itself albeit showing positive results on the anti-IgG assay. This reduced activity is due to the random, rather than directed binding of antibody to the activated AuNP surface. Therefore, a more rigorous method in preparing Ab-AuNP conjugates should be looked into.

3.3 Future Studies

The loading density and binding capacity of protein molecules onto AuNPs remain a big question to solve. The formation of these conjugates may seem simple, as it assumes a covalent bond using an organic linker (PEG chain) to bridge them, forming a protein-PEG-AuNP macromolecule, without focusing on a site-specific conjugation which requires greater technicality and precision in the chemistry. However, it is also important to ensure that a protein-AuNP molecule has greater activity than its single biomolecule to preserve its practicality as a biosensor. More importantly, the stability of these conjugates should remain a main priority in the rationale design of such biosensors.

As such, several confirmation and characterisation methods should be performed on the prepared conjugates especially XPS and TGA analysis, alongside TEM images which could confirm the conformation of such protein-AuNP conjugates. The more sophisticated characterisation can give greater understanding on the biomolecule orientation and the importance of protein to nanoparticle ratio in order to synthesise a well-defined conjugate and avoid aggregation of conjugates through non-specific

interactions. Furthermore, the optimal conjugation time for different classes of proteins (in this case, lectins and antibodies, and possibly be extended) should be determined exclusively so that various classes of biosensor can boast their maximum efficiency as biosensors.

To our knowledge, a simple, scalable and practical preparation of protein-AuNP conjugate has yet to be achieved. Many researches have targeted the investigations of site-specific conjugation of Abs and hence overlooked the simplicity behind the engineering of such biosensors. Therefore, this study serves as a proof of principle study towards a more economical and straight-forward construct of such conjugates which could open up many doors for the application in biological and medical fields, especially in diagnosis.

4. Materials and Methods

General procedures. All synthetic steps were carried out in room temperature. IR spectra were recorded on a Bruker ALPHA FTIR spectrometer as solid samples unless otherwise stated. UV/Vis spectra were recorded on a BioTek Synergy HT multi-detection microplate reader. Nanoparticle size measurements were characterised by dynamic light scattering (DLS) which was performed on a Malvern Instruments Zetasizer Nano-ZS. The starting material 40 nm gold colloid solution was purchased from BBI Solutions. PEG-2-mercaptoethylether acetic acid (PEGCOOH, M_n 3500), Corning® 96 well clear flat bottom polystyrene Carbo-BIND™ microplates, aniline (99.5 % ACS reagent), D-(+)mannose, α-D-glucose, D-(+)galactose, phosphate buffered saline (PBS) tablets, bovine serum albumin (BSA), mannan from *Saccharomyces cerevisiae* and MES monohydrate were purchased from Sigma-Aldrich. 100 mM acetate buffer with 1 mM aniline (pH 5.5) was prepared in 200 mL of Milli-Q water (with a resistance >19 mOhms). 100 mM MES buffer (pH 5.0) was prepared in 200 mL of Milli-Q water (with a resistance >19 mOhms). 10 mM HEPES buffer containing 0.05 M NaCl, 0.1 mM $CaCl_2$ and 0.01 mM $MnCl_2$ (pH 7.5, HEPES) was prepared in 200 mL of Milli-Q water (with resistance >19 mOhms). Unconjugated Peanut agglutinin from *Arachis hypogea* (PNA), *Dolichos biflorus* agglutinin (DBA) and Concanavalin A (Con A) were purchased from Vector Labs. Easy-Titer Rabbit IgG Assay Kit was purchased from Thermo Scientific and IgG from rabbit serum was purchased from Sigma-Aldrich.

Functionalisation of gold nanoparticles with PEG-2-mercaptoethylether acetic acid. PEG-2-mercaptoethylether acetic acid (1.0 mg) was dissolved in 40 nm gold nanoparticle dispersion (1.0 mL, 60 μg of gold, 0.3 μmol of gold) in a 1.5 mL Eppendorf tube. The mixture was incubated at RT for 30 min. The nanoparticles were purified in a centrifuge filter (Amicon Ultra 0.5 mL, 30 kDa) using centrifugation at 10000 rpm for 10 min. The particles were washed in the centrifuge filter with Milli-Q water (resistance >19 mOhms) (3 x 300 μL) before being re-dispersed in a final volume of 1.0 mL Milli-Q water in an Eppendorf and stored in the fridge until required.

Stability of PEGylated gold nanoparticles in sodium chloride, NaCl solution and PBS buffer. Sodium chloride (NaCl, 0.58 g, 10 mmol) was dissolved in pure water (10

mL) to obtain 1 M NaCl solution. 1 M NaCl solution was diluted with final concentrations used for testing in the range of 0.02 M to 1 M. PBS buffer (0.01 M) was diluted with final concentrations used for testing in the range of 0.16 mM to 10 mM. To both solutions, PEGylated gold nanoparticles (20 μL, 1.2 μg of gold, 0.36 nmol of gold) was added and mixed well. The mixture was incubated at RT for 30 min. Absorbance at 450 nm to 700 nm were measured. The change in colour of the solution was also noted.

Activation of PEGylated gold nanoparticles. A fresh solution of *N*-hydroxysuccinimide (10 mg, 90 μmol) and 1-Ethyl-3-(3-dimethylaminopropyl)carbodiimide hydrochloride (10 mg, 60 μmol) was prepared in 100 mM MES buffer (pH 5.0) was prepared. To the PEGylated gold particle dispersion in 100 mM MES buffer (pH 5.0) (100 μL, 60 μg of gold, 0.3 μmol of gold), the fresh activation solution (25 μL) was added and mixed well in a 1.5 mL Eppendorf tube. The mixture was incubated at RT for 30 min. Excess activation agents were removed by repeated washing with cold MES buffer (3 x 300 μL) in centrifuge filters (Amicon Ultra 0.5 mL, 30 kDa) using centrifugation at 11500 rpm for 5 min, spinning down to no more than 25 μL each time.

Preparation of protein-gold conjugates. Several protein solutions (BSA, PNA, DBA and Con A) of concentration 100 μg.mL^{-1} in cold PBS buffer were prepared. To the activated PEGylated gold nanoparticle solution (25 μL, 60 μg of gold, 0.3 μmol of gold), the protein solution in cold PBS buffer (300 μL) was added and mixed well. The mixture was incubated at RT for 4 h. The protein-gold conjugates were spun down to 25 μL in centrifuge filters (Amicon Ultra 0.5 mL, 30 kDa) using centrifugation at 11500 rpm for 5 min and washed with cold PBS buffer (1 x 300 μL). The conjugates were re-suspended in cold HEPES buffer (50 μL) and used immediately in assays.

Preparation of glycosylated surfaces. 30 mM monosaccharide solutions were prepared in 100 mM acetate buffer with 1 mM aniline. 100 μL of monosaccharide solution was then added to every well of a hydrazide functionalised 96 well microtitre plate before incubation at 50 ˚C for 24 h. After incubation, wells were extensively washed three times with Milli-Q water before being allowed to dry. Plates were

functionalised with mannose, glucose and galactose and were either used immediately or stored at -20 ˚C.

Carbohydrate binding assays. The protein-gold conjugates (BSA, PNA, DBA and Con A) were diluted with 10 mM HEPES with 0.15 M NaCl, 0.1 mM $CaCl_2$ and 0.01 mM $MnCl_2$ (pH 7.5) with final concentrations used for assay in the range of 0.90 $mg.mL^{-1}$ to 60 $mg.mL^{-1}$. 50 μL of the conjugates were then added to each well of a glycosylated plate before incubation at room temperature for 30 mins. After incubation, each well was rigorously washed 3 times with Milli-Q water before absorbance at 450 to 700 nm were measured. Each sample was analysed in triplicate.

Surface functionalisation analysis. 2 μL droplet of 1 $mg.mL^{-1}$ resorufin in water was added to the surface of the well. A picture of the droplet inside the well was taken using a smartphone. The image was imported into ImageJ (version 1.49) and the surface area of the well covered by the droplet was determined by drawing regions of interest around the well and the droplet. The area of the droplet region with respect to the area of the well region was converted into a percentage.

Kinetic studies on conjugation time of protein onto gold nanoparticles. 10 μL of 100 $\mu g.mL^{-1}$ mannan from *Saccharomyces cerevisiae* in 10 mM HEPES with 0.15 M NaCl, 0.1 mM $CaCl_2$ and 0.01 mM $MnCl_2$ (pH 7.5) was added to every well of a 384 well microtitre plate. 10 μL of gold conjugates incubated with Con A (300 μL, 100 $\mu g.mL^{-1}$) for different time periods (t = 0, 1, 2, 3, 4 h and overnight) were added to each well. The plate was incubated at RT for 30 min on a plate mixer to ensure proper mixing. Absorbance at 450 to 700 nm were measured. The change in colour of solution was also noted.

Preparation of antibody-gold conjugates. IgG solution of concentration 100 $\mu g.mL^{-1}$ in cold PBS buffer was prepared. To the activated PEGylated gold nanoparticle solution (25 μL, 60 μg of gold, 0.3 μmol of gold), the IgG solution in cold PBS buffer (300 μL) was added and mixed well. The mixture was incubated at RT for 4 h. The antibody-gold conjugates were spun down to 25 μL in centrifuge filters (Amicon Ultra 0.5 mL, 30 kDa) using centrifugation at 11500 rpm for 5 min and washed with cold PBS buffer (1 x

300 μL). The conjugates were re-suspended in cold PBS buffer (50 μL) and used immediately in assays.

Antibody binding assay. Antibody-gold conjugates were diluted with Easy-Titer® Dilution Buffer with final concentrations used for assay in the range of 0.90 mg.mL^{-1} to 60 mg.mL^{-1}. Anti-IgG sensitised beads were then treated with the indicated concentrations of conjugates, and incubated at RT for 10 min under vigorous mixing conditions, after which, 100 μL of Easy-Titer® Blocking Buffer was added to each well. This was then left at RT for 5 min under mixing at low speed. The absorbance at 405 nm was then measured. The IgG concentration of the original sample relative to the control sample was calculated. Each sample was analysed in triplicate. Negative control was PEGylated AuNP sample. Control samples were known concentrations of IgG solution in the range of 15.6 mg.mL^{-1} to 500 mg.mL^{-1}. Standard curves with intrapolation were generated using OriginPro 2016 (Academic) software.

5. References

1. Protein Interaction Networks, https://www.informatik.hu-berlin.de/de/forschung/gebiete/wbi/teaching/archive/ws1011/vl_bioinf/09_protein_interaction_networks.pdf, (accessed January 2016).

2. Thermo Scientific Pierce Protein Interaction Technical Handbook, https://tools.thermofisher.com/content/sfs/brochures/1601945-Protein-Interactions-Handbook.pdf, (accessed January 2016).

3. J. Westermarck, J. Ivaska and G. L. Corthais, *Mol. Cell. Proteomics*, 2013, **12**, 1752 – 1763.

4. E. M. Phizicky and S. Fields, *Microbiol. Rev.*, 1995, **59**, 94 – 123.

5. T. Bergård, S. Linse and P. James, *Proteomics*, 2007, **7**, 2833 – 2842.

6. L. M. Brettner and J. Masel, *BMC Syst. Biol.* 2012, **6**, 1 – 10.

7. K. H. Young, *Biol. Reprod.*, 1998, **58**, 302 – 311.

8. S. J. Wodak, J. Vlasbom, A. L. Turinsky and S. Pu, *Curr. Opin. Struct. Biol.*, 2013, **23**, 941 – 953.

9. C. M. Deane, L. Salwińsku, I. Xenarios and D. Eisenberg, *Mol. Cell. Proteomics*, 2002, **1**, 349 – 356.

10. C. A. Mirkin, R. L. Letsinger, R. C. Mucic and J. J. Storhoff, *Nature*, 1996, **382**, 607 – 609.

11. S. J. Hurst, A. K. R. Lytton-Jean and C. A. Mirkin, *Anal. Chem.*, 2006, **78**, 8313-8318.

12. N. L. Rosi, D. A. Giljohann, C. S. Thaxton, A. K. R. Lytton-Jean, M. S. Han and C. A. Mirkin, *Science*, 2006, **312**, 1027 – 1030.

13. D. S. Seferos, D. A. Giljohann, H. D. Hill, A. E. Prigodich and C. A. Mirkin, *J. Am. Chem. Soc.*, 2007, **129**, 15477 – 15479.

14. D. G. Georganopoulou, L. Chang, J-M. Nam, C. S. Traxton, E. J. Mufson, W. L. Klein and C. A. Mirkin, *Proc. Natl. Acad. Sci. U.S.A.*, 2005, **102**, 2273 – 2276.

15. W. P. Faulk and G. M. Taylor, *Immunochemistry*, 1971, **8**, 1081 – 1083.

16. J. M. Robinson, T. Takizawa, D. D. Vandré and R. W. Burry, *Microsc. Res. Techniq.*, 1998, **42**, 13 – 23.

17. O. V. Laere, L. De Wael and J. De Mey, *Histochemistry*, 1985, **83**, 397 – 399.

18. W. Eck, G. Craig, A. Sigdel, g. Ritter, L. J. Old, L. Tang, M. F. Brennan, P. J. Allen and M. D. Mason, *ACS Nano*, 2008, **2**, 2263 – 2272.

19. N. A. Staines, J. Brostoff and K. James, *Introducing Immunology*, Mosby-Yearbook, London, 2nd edn., 1993.

20. C. A. Janeway, P. Travers, M. Walport and M. J. Shlomchik, *Immunobiology: The Immune System in Health and Disease*, Garland Science, New York, 5th edn., 2001.

21. J. H. W. Leuvering, B. C. Goverde, P. J. M. thal and A. H. W. M. Schuurs, *J. Immunol. Methods*, 1983, **60**, 9 – 23.

22. L. A. Dykman and V. A. Bogatyrev, *Russ. Chem. Rev.*, 2007, **76**, 181 – 194.

23. V. Pavlov, Y. Xiao, B. Shiyahovsky and I. Willner, *J. Am. Chem. Soc.*, 2004, **126**, 11768 – 11769.

24. C. D. Medley, J. E. Smith, Z. Tang, Y. Wu, S. Bamrungsap and W. Tan, *Anal. Chem.*, 2008, **80**, 1067 – 1072.

25. A. Neely, C. Perry, B. Varisli, A. K. Singh, T. Arbneshi, D. Senapati, J. R. Kalluri and P. C. Ray, *ACS Nano*, 2009, **3**, 2834 – 2840.

26. L. R. Hirsch, R. J. Stafford, J. A. Bankson, S. R. Sershen, R. E. Price, J. D. Hazle, N. J. Halas and J. L. West, *Proc. Natl. Acad. Sci. U. S. A.*, 2003, **100**, 13549 – 13554.

27. V. P. Zharov, V. Galitovsky and M. Viegas, *Appl. Phys. Lett.*, 2003, **83**, 4897 – 4899.

28. G. E. Abraham, *Orig. Intern.*, 2008, **15**, 132 – 158.

29. G. F. Paciotti, L. Myer, D. Weinrich, D. Goia, N. Pavel, R. E. McLaughlin and L. Tamarkin, *Drug Deliv.*, 2004, **11**, 169 – 183.

30. G. F. Paciotti, D. G. I. Kingston and L. Tamarkin, *Drug, Dev. Res.*, 2006, **67**, 47 – 54.

31. L. A. Dykman and N. G. Khlebtsov, *Acta Naturae*, 2011, **3**, 34 – 55.

32. L. G. Fernández, PhD Thesis, Autonomous University of Barcelona, 2013.

33. A. J. Di Pasqua, R. E. Mishler, Y. L. Ship, J. C. Dabrowiak and T. Asefa, *Mater. Lett.*, 2009, **63**, 1876 – 1879.

34. J. Ljungblad, MSc Thesis, Linköping University Institute of Technology , 2009.

35. C. A. C. Wolfe and D. S. Hage, *Anal. Biochem.*, 1995, **231**, 123 – 130.

36. D. E. Owens III and N. A. Peppas, *Int. J. Pharm.*, 2006, **307**, 93 – 102.

37. J. Gao, X. Huang, H. Liu, F. Zan and J. Ren, *Langmuir*, 2012, **28**, 4464 – 4471.

38. W. Poon, X. Zhang, D. Bekah, J. G. Teodoro and J. L. Nadeau, *Nanotechnology*, 2015, **26**, DOI: 10.1088/0957-4484/26/28/285101.

39. J. Condem A, Ambrosone, v. Sanz, Y. Hernandez, V. Marchesano, F. Tian, H. Child, C. C. Berry, M. R. Ibarra, P. V. Baptista, C. Tortiglione and J. M. dela Fuente, *ACS Nano*, 2012, **6**, 8316 – 8324.

40. M. T. Peracchia, *S. T. P. Pharma. Sci.*, 2003, **13**, 155 – 161.

41. M. Faraday, *Philos. Trans. R. Soc. London*, 1857, **147**, 145 – 181.

42. J. Turkevich, P. C. Stevenson and J. Hillier, *Discuss. Faraday Soc.*, 1951, **11**, 55 – 75.

43. M. Brust, M. Walker, D. Bethell, D. J. Schiffrin and R. Whyman, *Chem. Commun.*, 1994, **7**, 801 – 802.

44. S. D. Perrault and W. C. W. Chan, *J. Am. Chem. Soc.*, 2009, **131** (47), 17042 – 17043.

45. M. N. Martin, J. I. Basham, P. Chando and S-K. Eah, *Langmuir*, 2010, **26** (10), 7410 – 7417.

46. E. Petryayeva and U. J. Krull, *Anal. Chim. Acta*, 2011, **706** (1), 8 – 24.

47. X. Liu, M. Atwater, J. Wang and Q. Huo, *Colloids Surf., B*, 2007, **58**, 3 – 7.

48. S-J. Richards and M. I. Gibson, *ACS Macro Lett.*, 2014, **3**, 1004 – 1008.

49. B. Bhushan, *Springer Handbook of Nanotechnology*, Springer, New York, U.S.A., 3rd edn., 2007, pp. 293 – 296.

50. *Nanotechnology for Cancer Therapy*, ed. M. M. Amiji, CRC Press, U.S.A., 2007, pp. 301 – 304.

51. M. I. Gibson, M. Danial and H-A. Klok, *ACS Comb. Sci.*, 2011, **13**, 286 – 297.

52. S. K. Vashist, *Diagnostics*, 2012, **2**, 23 – 33.

53. *Proteins and Nucleic Acids: The Biochemistry of Plants*, ed. A. Marcus, Academic Press, New York, U. S. A., Vol. 6, 1981, pp. 401 – 402.

54. L. Otten and M. I. Gibson, *RSC Adv.*, 2015, **5**, 53911 – 53914.

55. K. Godula and C. R. Bertozzi, *J. Am. Chem. Soc.*, 2010, **132**, 9963 – 9965.

56. B. Afrough, M. V. Dwek and P. Greenwell, *BioTechniques*, 2007, **43**, 458 – 464.

57. G. T. Hermanson, *Bioconjugate Techniques*, Academic Press, London, 3rd edn., 2013, pp. 211 – 212.

58. Department of Animal Science – Plants Poisonous to Livestock, http://poisonousplants.ansci.cornell.edu/toxicagents/lectins.html, (accessed May 2016).

59. J. Wang, D. Liu and Z. Wang, *Anal. Methods*, 2011, **3**, 1745 – 1751.

60. I. J. Goldstein, *J. Agric. Food Chem.*, 2002, **50**, 6583 – 6585.

61. K. A. Maupin, D. Liden and B. B. Haab, *Glycobiology*, 2012, **22**(1), 160 – 169.

62. V. Piller, F. Piller and J-P. Cartron, *Eur. J. Biochem.*, 1990, **191**, 461 – 466.

63. S. van der Heide and D. A. Russell, *J. Colloid Interface Sci.*, 2016, **471**, 127 – 135.

64. E, Casals, T. Pfaller, A. Duschi, G. J. Oostingh and V. Puntes, *ACS Nano*, 2010, **4**(7), 3623 – 3632.

65. Sigma-Alrich, Gold Nanoparticles: Properties and Applications, http://www.sigmaaldrich.com/materials-science/nanomaterials/gold-nanoparticles.html, (accessed May 2016).

6. Supplementary Information

6.1 Characterisation of AuNP Species

Characterisation data of various AuNP species in this report can be found in this section if not mentioned in the sections above.

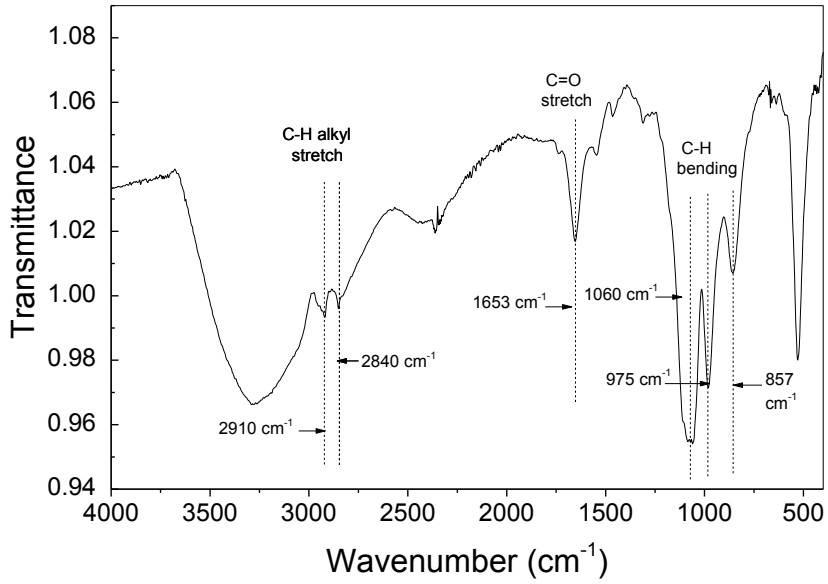

Figure S1. IR spectra of BSA-AuNP conjugate.

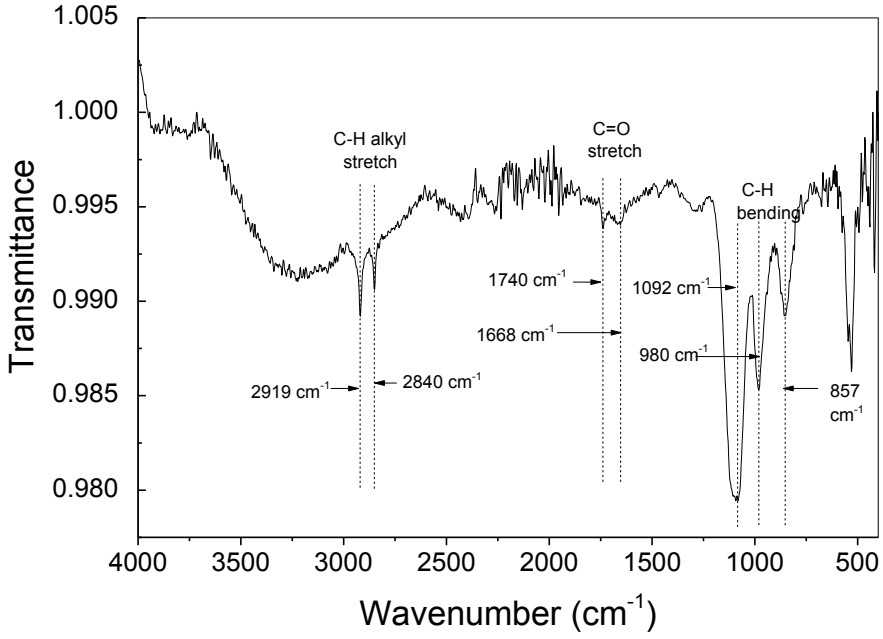

Figure S2. IR spectra of PNA-AuNP conjugate.

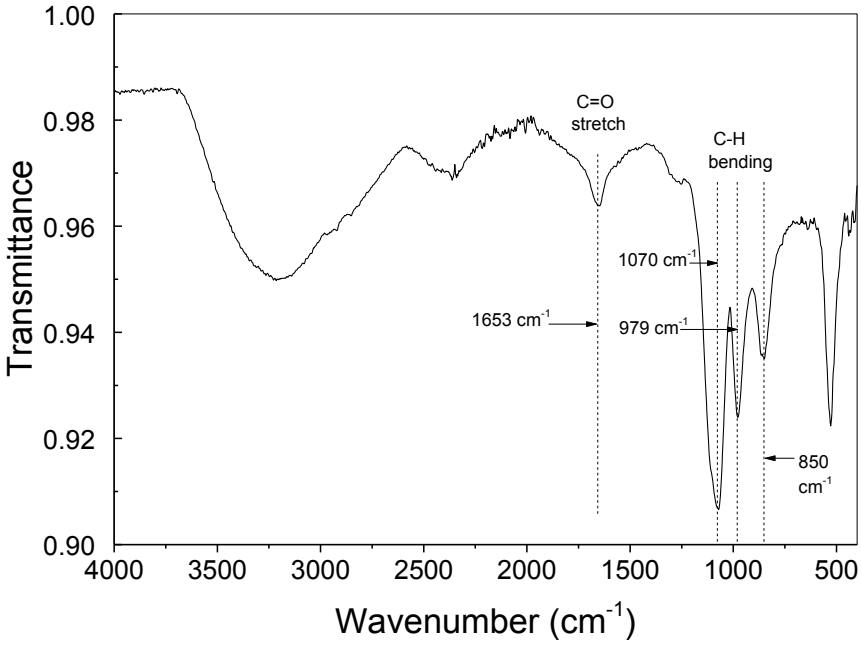

Figure S3. IR spectra of DBA-AuNP conjugate.

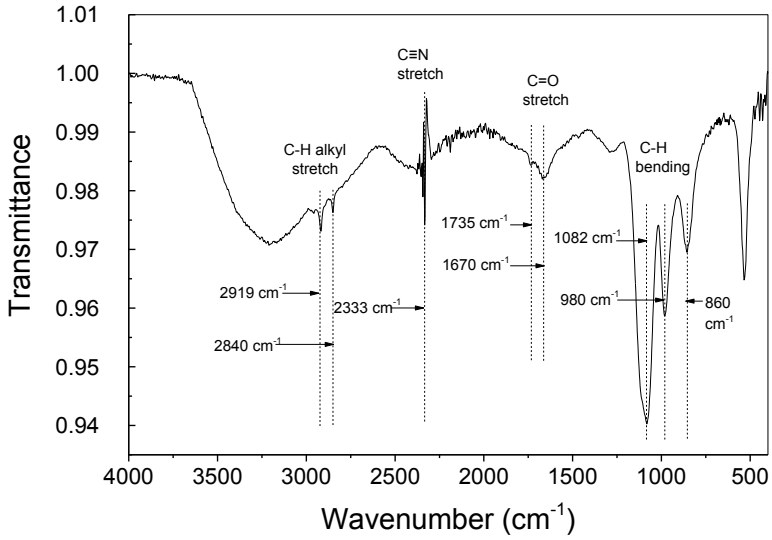

Figure S4. IR spectra of Con A-AuNP conjugate.

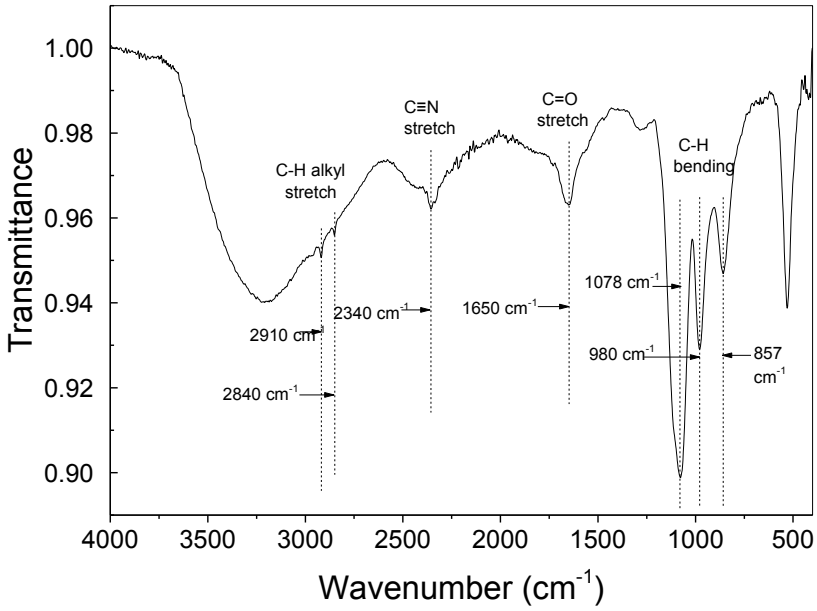

Figure S5. IR spectra of IgG-AuNP conjugate.

6.2 Stability of PEGylated AuNP in Saline Solution

6.2.1 UV/Vis Spectra of AuNP Species in NaCl Solution

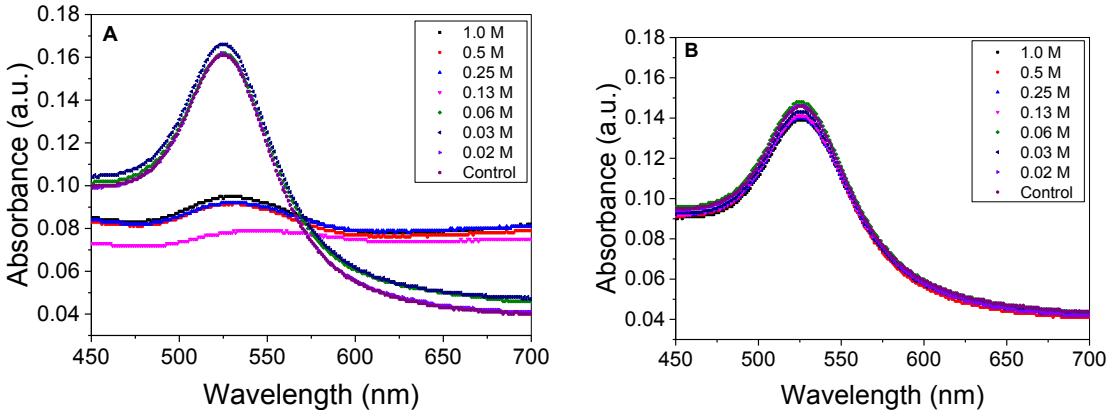

Figure S6. UV/Vis spectra of (A) 40 nm AuNP and (B) PEGylated AuNP in decreasing concentration of sodium chloride, NaCl solution.

6.2.2 UV/Vis Spectra of AuNP Species in PBS

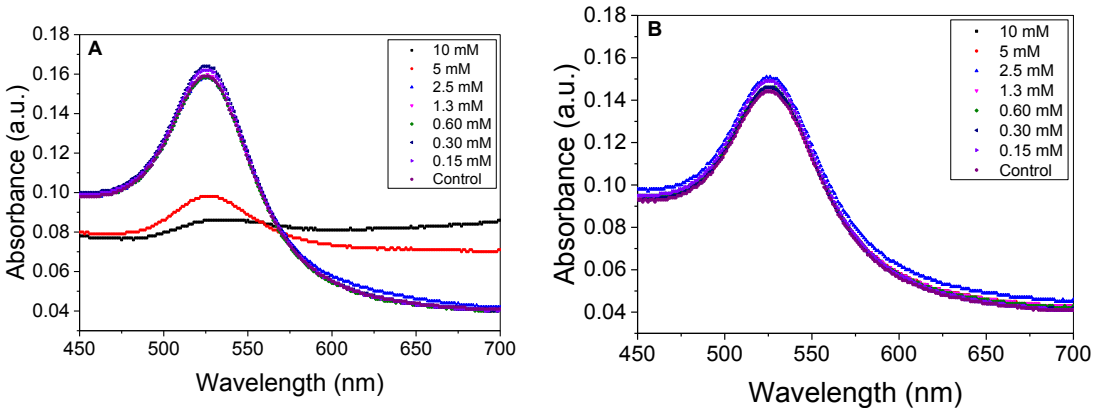

Figure S7. UV/Vis spectra of (A) 40 nm AuNP and (B) PEGylated AuNP in decreasing concentration of PBS.

6.3 Carbohydrate Binding Assays

6.3.1 UV/Vis Spectra for Galactose Binding Assay

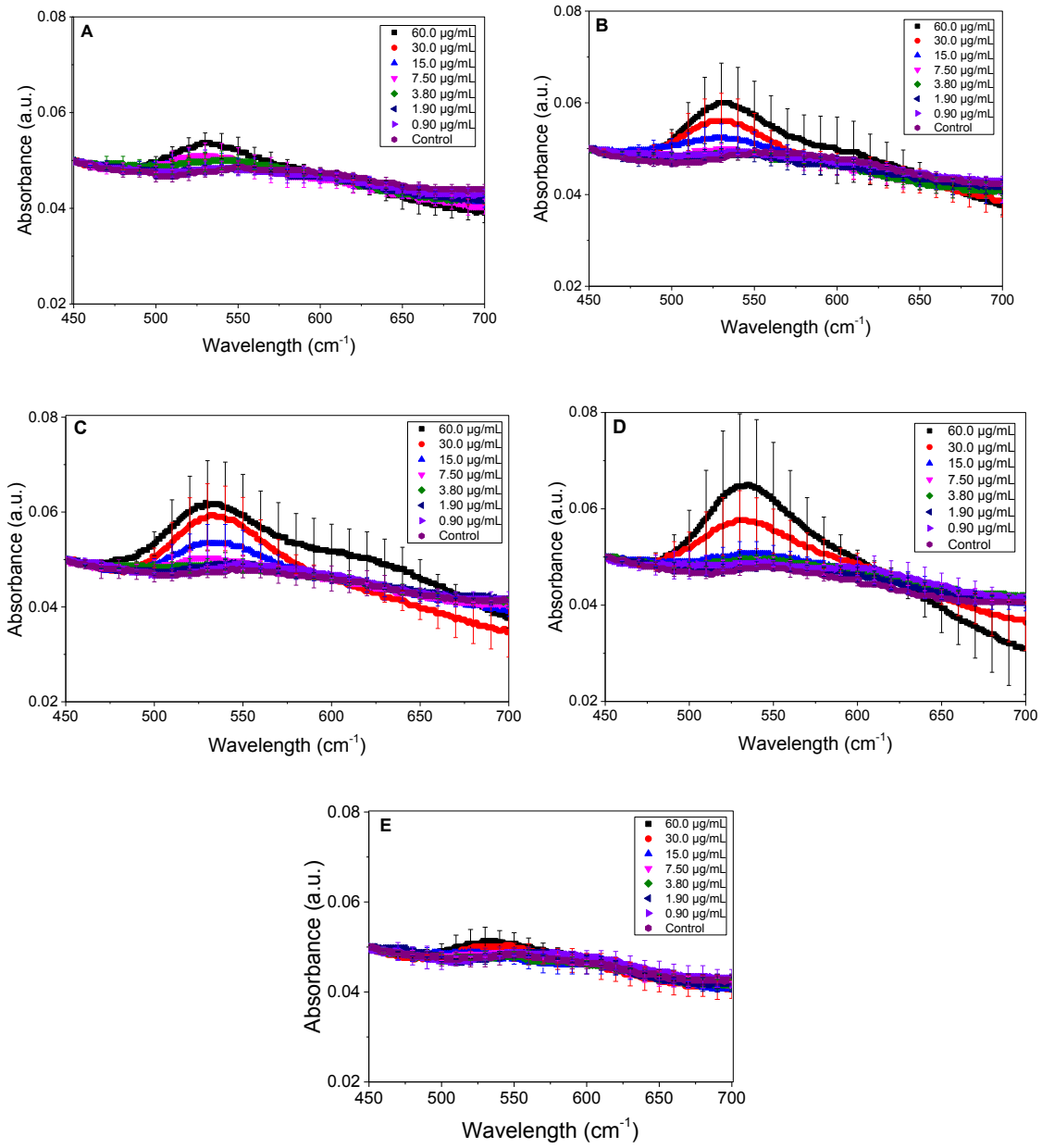

Figure S8. UV/Vis spectra for various AuNP conjugates in decreasing concentrations incubated with galactose surfaces at RT for 30 min; (A) BSA-AuNP, (B) PNA-AuNP, (C) DBA-AuNP, (D) Con A-AuNP and (E) PEGylated AuNP.

6.3.2 UV/Vis Spectra for Glucose Binding Assay

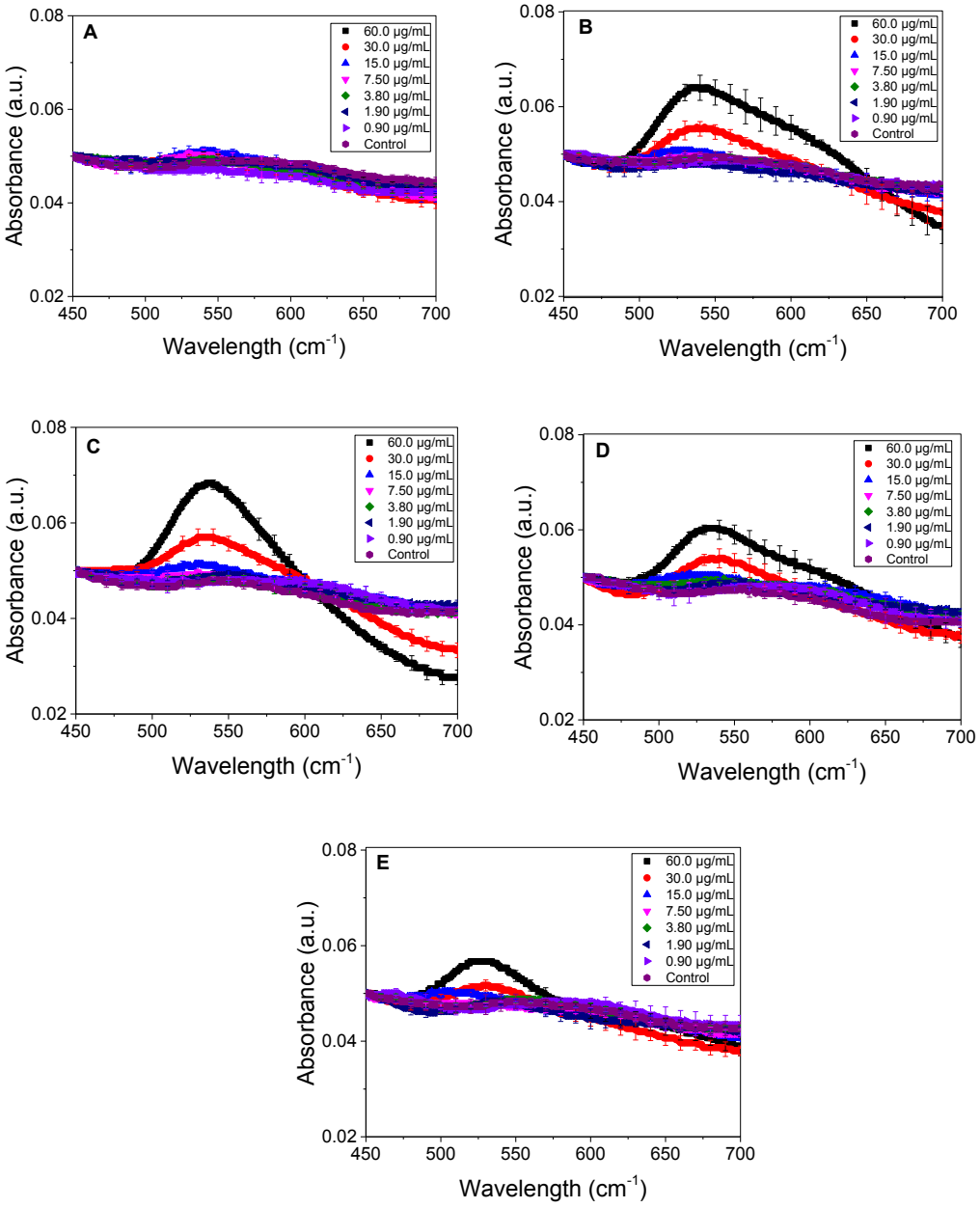

Figure S9. UV/Vis spectra for various AuNP conjugates in decreasing concentrations incubated with glucose surfaces at RT for 30 min; (A) BSA-AuNP, (B) PNA-AuNP, (C) DBA-AuNP, (D) Con A-AuNP and (E) PEGylated AuNP.

6.3.3 UV/Vis Spectra for Mannose Binding Assay

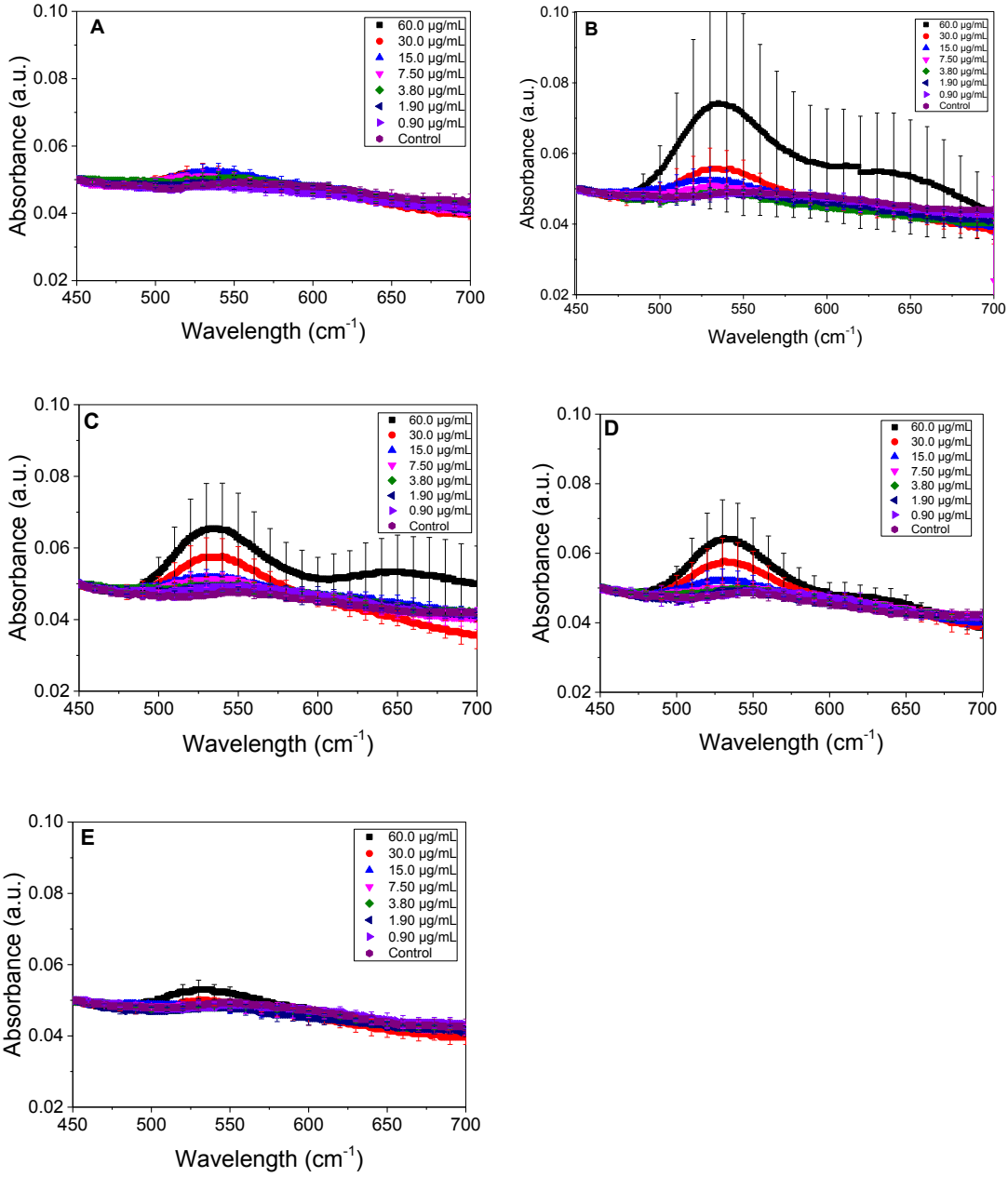

Figure S10. UV/Vis spectra for various AuNP conjugates in decreasing concentrations incubated with mannose surfaces at RT for 30 min; (A) BSA-AuNP, (B) PNA-AuNP, (C) DBA-AuNP, (D) Con A-AuNP and (E) PEGylated AuNP.